NASA/TM–2014-218259

Applying Pressure Sensitive Paint Technology to Rotor Blades

A. Neal Watkins, Bradley D. Leighty, and William E. Lipford
Langley Research Center, Hampton, Virginia

Kyle Z. Goodman
Analytical Mechanics Associates, Inc., Hampton, Virginia

Jim Crafton
Innovative Scientific Solutions, Inc., Dayton, Ohio

James W. Gregory
The Ohio State University, Columbus, Ohio

May 2014

NASA STI Program . . . in Profile

Since its founding, NASA has been dedicated to the advancement of aeronautics and space science. The NASA scientific and technical information (STI) program plays a key part in helping NASA maintain this important role.

The NASA STI program operates under the auspices of the Agency Chief Information Officer. It collects, organizes, provides for archiving, and disseminates NASA's STI. The NASA STI program provides access to the NASA Aeronautics and Space Database and its public interface, the NASA Technical Report Server, thus providing one of the largest collections of aeronautical and space science STI in the world. Results are published in both non-NASA channels and by NASA in the NASA STI Report Series, which includes the following report types:

- TECHNICAL PUBLICATION. Reports of completed research or a major significant phase of research that present the results of NASA Programs and include extensive data or theoretical analysis. Includes compilations of significant scientific and technical data and information deemed to be of continuing reference value. NASA counterpart of peer-reviewed formal professional papers, but having less stringent limitations on manuscript length and extent of graphic presentations.

- TECHNICAL MEMORANDUM. Scientific and technical findings that are preliminary or of specialized interest, e.g., quick release reports, working papers, and bibliographies that contain minimal annotation. Does not contain extensive analysis.

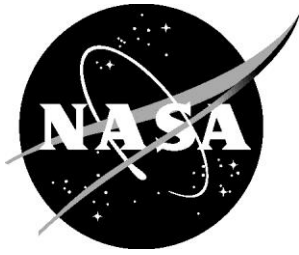- CONTRACTOR REPORT. Scientific and technical findings by NASA-sponsored contractors and grantees.

- CONFERENCE PUBLICATION. Collected papers from scientific and technical conferences, symposia, seminars, or other meetings sponsored or co-sponsored by NASA.

- SPECIAL PUBLICATION. Scientific, technical, or historical information from NASA programs, projects, and missions, often concerned with subjects having substantial public interest.

- TECHNICAL TRANSLATION. English-language translations of foreign scientific and technical material pertinent to NASA's mission.

Specialized services also include organizing and publishing research results, distributing specialized research announcements and feeds, providing information desk and personal search support, and enabling data exchange services.

For more information about the NASA STI program, see the following:

- Access the NASA STI program home page at *http://www.sti.nasa.gov*

- E-mail your question to help@sti.nasa.gov

- Fax your question to the NASA STI Information Desk at 443-757-5803

- Phone the NASA STI Information Desk at 443-757-5802

- Write to:
  STI Information Desk
  NASA Center for AeroSpace Information
  7115 Standard Drive
  Hanover, MD 21076-1320

Applying Pressure Sensitive Paint Technology to Rotor Blades

A. Neal Watkins, Bradley D. Leighty, and William E. Lipford
Langley Research Center, Hampton, Virginia

Kyle Z. Goodman
Analytical Mechanics Associates, Inc., Hampton, Virginia

Jim Crafton
Innovative Scientific Solutions, Inc., Dayton, Ohio

James W. Gregory
The Ohio State University, Columbus, Ohio

May 2014

Abstract

This report will present details of a Pressure Sensitive Paint (PSP) system for measuring global surface pressures on rotorcrtaft blades in simulated forward flight at the 14- by 22-Foot Subsonic Tunnel at the NASA Langley Research Center. The basics of the PSP method will be discussed and the modifications that were needed to extend this technology for use on rotor blades. Results from a series of tests will also be presented as well as several areas of improvement that have been identified and are currently being developed for future testing.

1. Introduction

The accurate determination of spatially continuous pressure and temperature distributions on aerodynamic surfaces is critical for the understanding of complex flow mechanisms and for comparison with computational fluid dynamics (CFD) predictions. Conventional pressure measurements are based on pressure taps and electronically scanned pressure transducers or embedded pressure transducers. While these approaches provide accurate pressure information, pressure taps/transducers are limited to providing data at discrete points. Moreover, the integration of a sufficient number of pressure taps/transducers on a surface can be time and labor intensive and expensive.

This is especially true in rotorcraft research, where the examination of pressure distributions on the blade is vital to advance analytical prediction methods for rotorcraft aerodynamics, acoustics, and interactional effects. There has been considerable research involving pressure measurements on rotor blades.[1-4] However, these measurements typically lack the spatial resolution necessary to capture phenomena such as the nascent tip vortex or dynamic stall. Instrumenting the blades with additional transducers to increase spatial resolution can quickly become prohibitive due to the cost and practicality of fitting a large number of sensors into a small area. In addition, the added centrifugal loads of the pressure transducers can rapidly become unmanageable.

The Pressure Sensitive Paint (PSP) technique may provide a means to non-intrusively measure the global surface pressures on these types of surfaces. Over the last several years, the U.S. Army Aeroflightdynamics Directorate, Joint Research Program Office, and the NASA Subsonic Rotary Wing Project have partnered to develop the PSP measurement technique for use on rotor blades. This work included an initial proof of concept work in 2003[5] which resulted in the development of instrumented pressure blades for more extended testing in 2008.[6] From these results, a new PSP system based on the previously described system was developed with several modifications for use with rotating test articles and successfully demonstrated for a rotorcraft in hover.[18] This report will detail these modifications as well as present results from the deployment of this system in the 14- by 22-Foot Subsonic Tunnel (hereafter abbreviated 14x22).

2. Pressure Sensitive Paint

Introduction to PSP

The PSP technique[7-11] exploits the oxygen (O_2) sensitivity of luminescent probe molecules suspended in gas-permeable binder materials. When a luminescent molecule absorbs a photon, it transitions to an excited singlet energy state. The molecule can then recover to the ground state by the emission of a photon of a longer wavelength, known as a radiative process. However, certain of these materials can also

interact with an O_2 molecule such that the transition back to the ground state is non-radiative in a process known as collisional quenching. The rate at which these two process (radiative vs. non-radiative) compete is dependent on the concentration of O_2 present and can be described by the Stern-Volmer relationship[12]

$$I_0 / I = 1 + K_{SV}(T)P_{O_2} \tag{1}$$

where I_0 is the luminescence intensity in the absence of O_2 (i.e. vacuum), I is the luminescence intensity at some partial pressure of oxygen P_{O2}, and K_{SV} is the Stern-Volmer constant, which is dependent on temperature (T).

There are several issues with this relationship, especially in regards to wind-tunnel applications; first, it is a practical impossibility to measure I_0 in a wind tunnel application. Second, the luminescent signal from the paint is not only a function of pressure; it also varies with factors such as illumination intensity, probe concentration, paint layer thickness, and detector sensitivity. These spatial variations typically result in a non-uniform luminescent signal from the painted surface. The spatial variations are usually eliminated by taking a ratio of the luminescent intensity of the paint at the test condition with the luminescent intensity of the paint at a known reference condition (usually wind-off). Thus Eq. 1 can be cast into a more suitable form
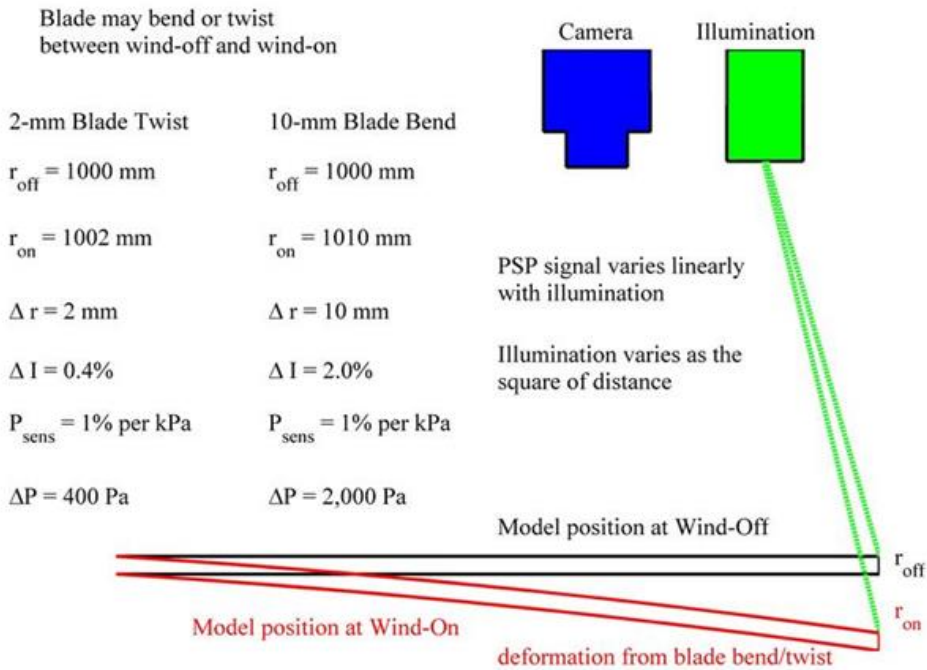
$$I_{REF} / I = A(T) + B(T) * (P / P_{REF}) \tag{2}$$

where I_{REF} is the recovered luminescence intensity at a reference pressure, P_{REF}. The coefficients $A(T)$ and $B(T)$ are temperature dependent constants for a given PSP formulation and are usually determined beforehand using laboratory calibration procedures.

Sources of Error in PSP Measurements for Rotor Blades

While there are several approaches to acquiring PSP data, each suffer from the same sources of error, which have been investigated and modeled by Liu.[11] These error sources include temperature, illumination, model displacement/deformation, sedimentation, photo-degradation of the luminophore, stray light, and camera shot noise. In the case of a helicopter rotor blade, illumination errors associated with model deformation (as caused by aeroelastic effects) are a significant source of error.

The relationship between surface illumination and paint luminescence is linear; thus, any change in surface illumination will result in an equal change in paint luminescence. Errors in pressure measurements caused by surface illumination variations can stem from several sources. An example of this with illumination from a point source is shown in Fig. 1. The relationship between illumination intensity at a point on the surface and the distance between the source and the point of interest are an inverse function of the distance squared. Any movement of the painted surface or illumination source will result in a change in the distance between these two points, thus causing a change in the illumination intensity at the surface. Using some common assumptions about the PSP, the example shown in Fig. 1 shows that for a modest change in the illumination field, there can be fairly large pressure errors. Moreover, this source of error can result from deformation of the model surface or physical displacement of the model or illumination source. Another source of illumination error is the temporal stability of the illumination source. Any variation of the intensity source between the wind-off (reference) and wind-on images will register as an error in illumination.

Blade may bend or twist
between wind-off and wind-on

Camera   Illumination

2-mm Blade Twist   10-mm Blade Bend

r_{off} = 1000 mm r_{off} = 1000 mm

r_{on} = 1002 mm r_{on} = 1010 mm

Δr = 2 mm Δr = 10 mm

ΔI = 0.4% ΔI = 2.0%

P_{sens} = 1% per kPa P_{sens} = 1% per kPa

ΔP = 400 Pa ΔP = 2,000 Pa

PSP signal varies linearly
with illumination

Illumination varies as the
square of distance

Model position at Wind-Off r_{off}

Model position at Wind-On r_{on}

deformation from blade bend/twist

Figure 1. Schematic of illumination errors in PSP measurements.

As described above, PSP is an intensity-based approach that requires the use of (at least) two images leading to the introduction of this type of error. For this work, a system capable of compensating for this error has been developed based on the lifetime-based method.

Lifetime-Based Pressure Sensitive Paint Measurements

For this work, the PSP data was acquired using a "lifetime-based" approach.[13-17] In the traditional lifetime-based technique, excitation of the PSP is accomplished using a modulated light source (e.g. laser, flash lamp, or pulsed LED arrays). A fast framing camera (intensified CCD or interline transfer CCD) is used to collect the excited state luminescence decay. Typically the decay is approximated by acquiring two or more images at different delay times during and/or after the pulsed excitation and integrating photons for fixed periods of time (i.e. gate widths) that have been predetermined to maximize the pressure sensitivity, as demonstrated in Fig. 2. The first image (Gate 1) usually consists of a short gate width and is collected either during the excitation pulse or shortly after it ends. This can be thought of as the reference image because the excited-state decay has the least pressure sensitivity. The second image (Gate 2) is taken at a later time after the excitation pulse and usually has a longer gate width, ensuring maximum pressure (and temperature) sensitivity. More information on this lifetime technique can be found in Watkins et al.[17]

Fast Responding Pressure Sensitive Paint

Typical paint formulations are comprised of an oxygen sensitive fluorescent dye and a binder to physically adhere the dye to the model surface. Conventional formulations typically use a polymer as a
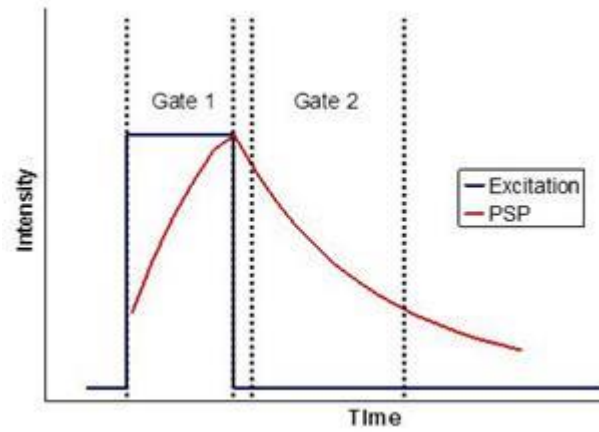
3

binder material. The disadvantage of the binder is that it inhibits interaction of atmospheric oxygen with the embedded dye molecules. The response time of the paint to pressure is largely governed by the rate of diffusion of gas into the binder. Conventional, polymer-based paint formulations have response times on the order of one second, making them unsuitable for evaluating unsteady aerodynamic phenomena. Aeroelastic and rotorcraft phenomena are inherently unsteady with frequency content of 10-Hz to 1,000-Hz, and therefore, conventional paint formulations are insufficient for the tests to be conducted in this program.

Figure 2. Schematic representation of lifetime-based data acquisition showing excitation (blue) and measured emission (red). The gate regions represent example Gate 1 (during excitation) and Gate 2 (after excitation).

The temporal response characteristics of pressure-sensitive paint are primarily governed by the thickness of the paint formulation and the diffusion coefficient of the binder material, according to the relation
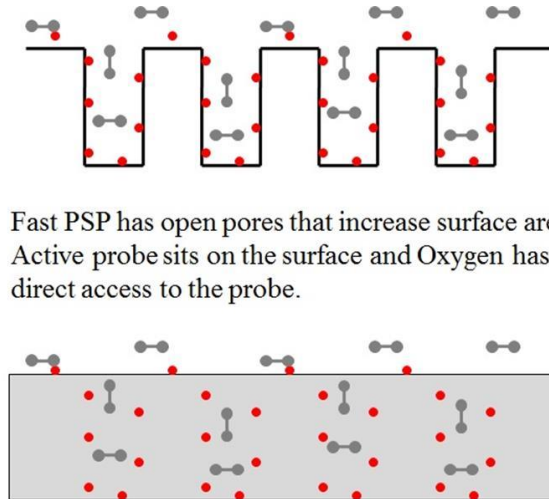
$$\tau_{diff} \propto h^2/D_m \tag{3}$$

where the response time due to diffusion (τ_{diff}) increases with the paint thickness (h) squared and decreases with increasing diffusion coefficient (D_m). Some investigators have focused on decreasing the thickness of the paint in order to improve the response characteristics. This approach, however, has the disadvantage of sacrificing luminescent output from the paint, and thus signal-to-noise ratio (SNR). The paint formulation used in this work has been developed based on the strategy of increasing the diffusivity of gas within the paint binder, as described by Gregory.[18] Porous binders have been developed with the goal of enhancing the oxygen diffusion within the paint layer and thus improving the temporal response characteristics.


Fast PSP has open pores that increase surface area. Active probe sits on the surface and Oxygen has direct access to the probe.

Regular PSP requires that the Oxygen diffuse through the binder to the active probe. The diffusion process is much slower.

Figure 3. Schematic difference between conventional PSP (bottom) and fast PSP (top).

The difference between conventional polymer-based PSP and a porous PSP is described schematically in Fig. 3. For conventional PSP, oxygen molecules in a test gas need to permeate into the binder layer for oxygen quenching. The process of oxygen permeation in a polymer binder layer produces slow response times for a conventional PSP. On the other hand, the dye in a

4

porous PSP is opened to the test gas so that the oxygen molecules are free to interact with the dye. The open binder creates a PSP that responds quickly to changes in oxygen concentration, and thus pressure. A large effective surface area due to porous surface improves luminescence intensity, and thus a higher SNR can be achieved. The drawback of the porous PSP approach is that the dye is too accessible to the oxygen. This results in near complete quenching of all dye molecules at very low pressures. These formulations are effective for supersonic tunnels where the static pressure is below 3-psia. For lower speed applications, the signal-to-noise ratio suffers.
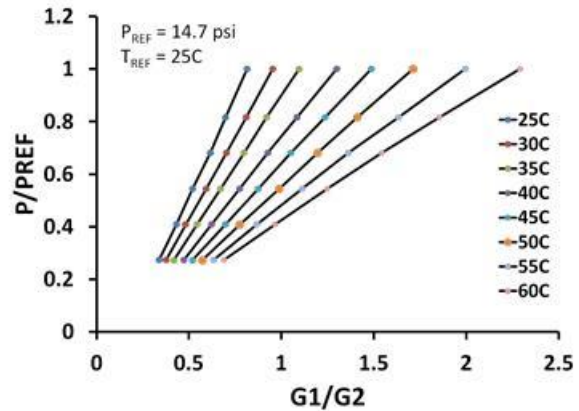
Figure 4. Calibration of PSP formulation for various temperatures and pressures.

Hybrid paint formulations have been developed that incorporate the advantages of both traditional and porous PSP. The resulting system is a fast time response paint layer with favorable signal-to-noise at higher pressure, and the paint can by air brushed onto a model. The polymer/ceramic formulation incorporates a high percentage of ceramic particles that provide the porous structure for rapid oxygen quenching, with a small amount of polymer to bind the paint to the surface. A dye molecule such as PtTFPP is deposited onto the polymer/ceramic surface to complete the paint formulation. Gregory and Sullivan[19] have used these polymer/ceramic PSP formulations to measure oscillating pressure fluctuations with frequencies up to 20-kHz. Porous polymer PSP has been used for unsteady pressure measurements on a turbocharger compressor blade,[20] model airplane propeller blades,[21] and rotorcraft blades.

Temperature Measurements on the Blade using TSP

Temperature sensitivity has long been a major source of error for PSP systems. The temperature sensitivity of the fast PP-PtTFPP PSP is quite high, as can be seen from the calibration in Fig. 4. Temperature sensitivity can be minimized and compensated for using a variety of tools such as isothermal models and in-situ transducer corrections. These tools are of limited value for the rotorcraft measurement as transducers are difficult to install and blade composition is driven by other issues. Uncertainty in the temperature of the blade is one of the most significant remaining errors in the fast PSP system. It is clear from the data acquired in previous tests that there are at least two major temperature variations to be dealt with, 1) a change in the blade bulk temperature between wind-off and wind-on as the tunnel heats up, and 2) a radial temperature gradient on the blade due to the local dynamic temperature.

Conceptually the addition of a TSP to the blade should be relatively simple; unfortunately there are several constraints that complicate the process. The TSP should operate using the same excitation and detection hardware used for the PSP, the single-shot lifetime system. An ideal TSP could be combined with the existing PSP to form a binary system; this would allow measurements of temperature at each location of the blade and therefore, local temperature variations caused by structures in the blade could be identified and corrected.

3. Experimental

Paint Formulation and Calibration

For making PSP measurements, the blades were coated with a porous polymer formulation described above. The oxygen sensitive luminophore chosen was platinum meso-tetrakis(pentafluorophenyl) porphine (abbreviated Pt(TfPP)), which is a common luminophore for PSP applications. A typical application of the PSP involved initially applying the porous polymer binder to a basecoat (usually white to maximize intensity collection efficiency) using conventional spraying techniques. After the binder dries, a solution of the luminophore is then typically over-sprayed onto the binder. This helps to ensure that the luminophore is resting on the surface for maximum interaction with oxygen (thus increasing the frequency response). The disadvantage of this is that the luminophore can degrade fairly quickly. However, this can be alleviated by simply over-spraying with additional luminophore solution. For this work, it was found that over-spraying once a day before running was sufficient for data acquisition.

Calibration of the paint formulation was performed separate from the wind tunnel in a laboratory calibration chamber. This chamber is only capable of measuring pressure and temperature sensitivities; no attempt to determine the frequency response of this paint was attempted. However, as mentioned above, previous testing has shown that this formulation can respond to 5 kHz, well above the frequency range needed for this test. For calibrations, the PSP was applied to 3-inch diameter aluminum coupons that were then placed in the calibration chamber. Illumination of the PSP and acquisition of the luminescent intensity was accomplished using the same system as used in the tunnel.

The PSP formulation was calibrated over a pressure range of 41 to 101 kPa (6 to 14.7 psia) at temperature ranging from 25 to 60 $^{\circ}$C (77 to 140 $^{\circ}$F). A calibration model for the coating was derived by solving Eq. (2) for normalized pressure in terms of the normalized temperature and the gate intensities acquired from the images as described in the previous section. The calibration data showed a multi-dimensional dependence on both pressure and temperature, which can be attributed to the complex nature of oxygen diffusion into the paint binder.[9-11] A linear least squares algorithm was used to fit the data to a modified and expanded version of Eq. (2) above assuming a second order relationship in both temperature and pressure

$$\begin{aligned}
(P/P_{REF}) = &(a_{11} + a_{12}(T/T_{REF}) + a_{13}(T/T_{REF})^2) + \\
&(a_{21} + a_{22}(T/T_{REF}) + a_{23}(T/T_{REF})^2)(G_1/G_2) + \\
&(a_{31} + a_{32}(T/T_{REF}) + a_{33}(T/T_{REF})^2)(G_1/G_2)^2
\end{aligned} \tag{4}$$

where P and P_{REF} are the pressures, T and T_{REF} are the temperatures, G_1 and G_2 are the intensities in the respective gates (analogous to I_{REF} [$G1$] and I [$G2$]), and a_{xy} are the calibration coefficients. A typical calibration is shown in Fig. 4.

For the temperature measurements, the TSP was formulated based on the same porous polymer binder. However, instead of employing Pt(TfPP) as the luminophore, a ruthenium complex was used instead. In the porous polymer binder, the ruthenium showed little pressure sensitivity with an easily measured temperature sensitivity. In addition, its excited state lifetime was found to be similar to the Pt(TfPP), thus allowing a similar timing scheme to be used with each paint. For this work, the TSP sensitivity was found to be linear in the range of 15-55 $^{\circ}$C with a sensitivity of 2.85%/$^{\circ}$C.
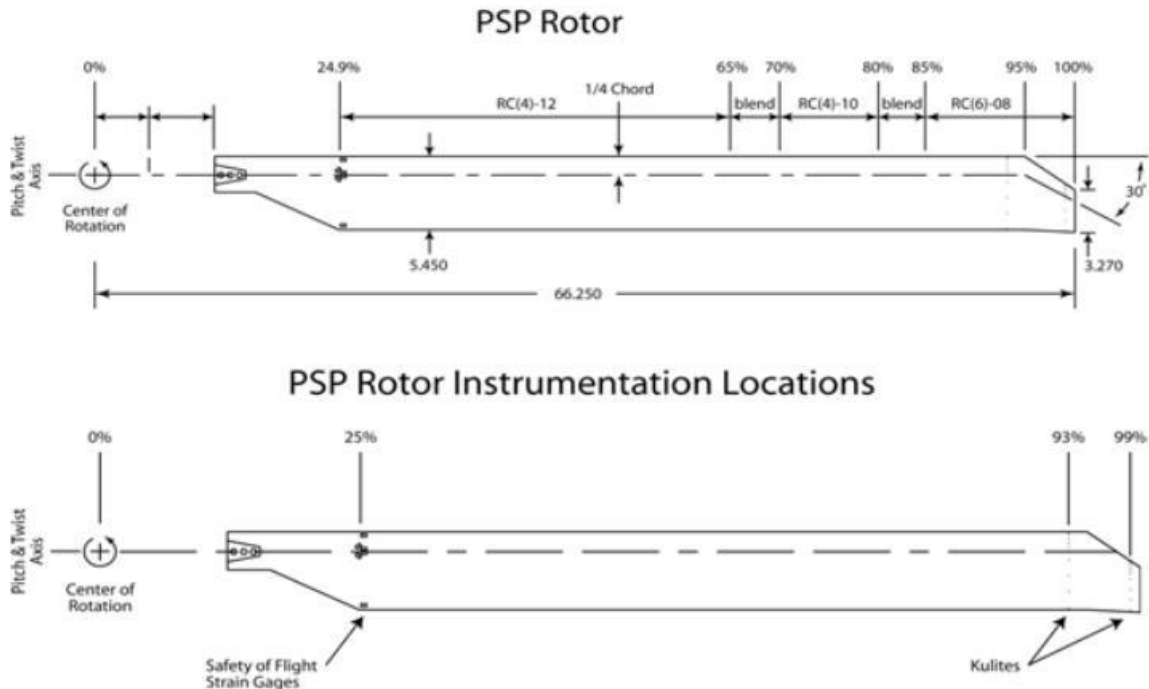
Figure 5. Rotor blades for use with PSP. The upper diagram shows the distribution of the airfoils and the dimensions of the blades (in inches). The lower diagram shows the rotor instrumentation locations.

Model and Facilities

The rotor blades that were tested have been constructed from carbon fiber, fiberglass, and aromatic nylon fiber honeycomb trailing-edge core. Each blade has been painted with a white basecoat to enhance the PSP luminescent output (by scattering the luminescence away from the surface and back to the camera) as well as to seal the blade to protect the blade structure from the solvents used in the painting process. The blades are constant chord with a swept-tapered tip and a 14 degree linear twist distribution, using the RC family of airfoils.[22-23] The upper portion of Fig. 3 shows the distribution of airfoils and the dimensions of the blades (in inches). Of the four blades, two are pressure instrumented using Kulite pressure sensors. The first instrumented blade has two rows of chord-wise transducers, with rows located at the 93% and 99% radial stations. The second has one chord-wise row at 93% radius. Each row has 10 pressure transducers located on the upper surface, as shown in the lower portion of Fig. 5.

The forward flight testing was conducted in the 14x22 facility at NASA Langley Research Center. The tunnel is an atmospheric, closed return tunnel with a test section 4.4 m (14.5 ft) high, 6.6 m (21.75 ft) wide, and 15.2 m (50 ft) long. The tunnel can reach a maximum velocity of 106 m/s (348 ft/s) with a dynamic pressure of 6.9 kPa (144 psf). The achievable Reynolds number of the tunnel ranges from 0 to 7.2×10^6 per meter (0 to 2.2×10^6 per foot). Test section airflow is produced by a 12.2 m (40 ft) 9 bladed fan driven by an 8.9 MW (12,000 Hp) main drive.

The rotor blades were mounted to the General Rotor Model System (GRMS) and a modified ROtor Body INteraction (ROBIN) fuselage. GRMS is a generic rotor drive system that allows testing of different rotor and fuselage configurations. GRMS is powered by two 55.9 kW (75 Hp) water-cooled electric motors that
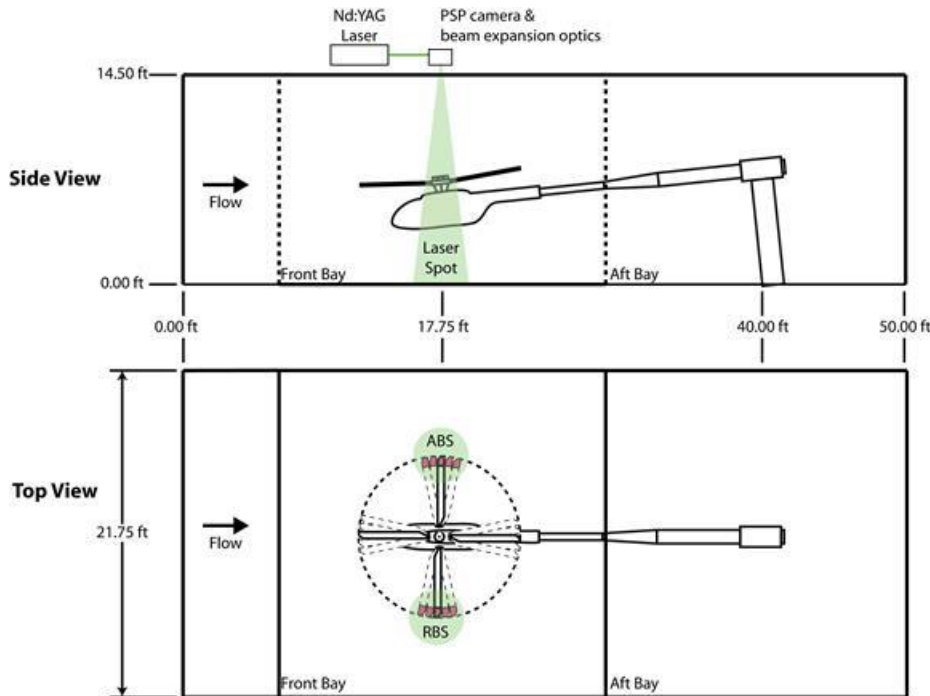
Figure 6. Wind tunnel configuration of model with instrumentation for first entry. The measurement locations are depicted in the lower image.

drive a 5.47:1 transmission. Two six component strain gage force and moment balances are contained within GRMS to enable separate measurement of rotor and fuselage loads. The rotor hub is a four bladed fully articulated hub. One blade cuff is instrumented to measure cuff pitch, lead lag, and flapping. Additional instrumentation on GRMS includes an encoder to provide 1/rev and 1024/rev timing signals and accelerometers to monitor machine health. The fuselage is similar to the original ROBIN fuselage with the exception of a rear ramp section. The ROBIN fuselage is an analytically defined representative generic helicopter fuselage that has been used in previous work.[24]

The modified ROBIN fuselage used in this test uses the same family of super-ellipse equations as the original ROBIN fuselage while employing a modified set of coefficients to generate the ramp section.

All PSP instrumentation was mounted on the ceiling of the 14x22 so that illumination and image acquisition were performed though Acrylite™ OP-4 windows. OP-4 is a brand of acrylic plastic that can transmit UV light. It also has a high clarity, transmitting ~90% of visible light. Two instrumentation/illumination packages were mounted above the test section ceiling to enable measurements at two locations on the rotor disk. For the first test entry in which only the last 10% of the blade was painted near the tip, data was collected when the blade was on the Advancing Blade Side (ABS) and on the Retreating Blade Side (RBS) as shown in Fig. 6. During the second test entry, the entire upper surface of the blade was painted and the instrumentation/illumination packages were placed to image the blades directly over the tail and on the RBS.

Instrumentation

Illumination for this work was provided by a series of frequency doubled Nd:YAG lasers (532 nm). A laser-based illumination system was used to attempt to acquire the PSP images needed in one single laser pulse as opposed to several hundred LED flashes (with one flash per revolution). This would provide instantaneous pressure data on the blade while also alleviating issues with the dynamic nature of rotorcraft flight (i.e. blade lead-lag and flap motion). The laser employed was a rugged, compact dual laser head system originally designed for Particle Image Velocimetry (PIV) applications. Because of this, the lasers have been pre-aligned so that the laser path from each head is co-linear and the timing can be manipulated so that both heads fire at nearly the same time (though a slight delay of ~ 20ns is needed to achieve maximum power[25]). The lasers employed had a nominal power of 200 mJ per pulse per head.

For the first test entry, PCO1600 cameras were used for data collection. The PCO1600 is a specialized interline transfer camera developed specifically for use in PIV applications and operated by masking every other line of the chip, allowing for charge to be transferred quickly (~200 ns transfer time) from the unmasked to the masked region for either storage or readout. This allows for the rapid collection of image pairs with a minimal time delay between images (the interline transfer time above). The camera employs a CCD chip with an active area of 1600 x 1200 pixels with peak quantum efficiency greater than 50% at 650 nm. The camera has 14-bit digitization as well as on-board memory that will allow it to rapidly store images on the camera, making it possible to run multiple cameras simultaneously from the same computer platform. However, the main limitation of the PCO1600 is that it employs a 100 ns clock, resulting in this amount of timing jitter when the camera is triggered externally. If only one camera is needed for imaging (as in the case of the first tunnel entry), this is not an issue. Unfortunately, multiple cameras were needed to image the entire upper surface of the blade in the second entry (3 cameras at the RBS and 2 cameras over the tail).

For the second entry, a new camera system was designed that incorporated the same interline transfer CCD chip employed in the PCO1600 but was driven using a clock with an accuracy greater than 10 ns, resulting in significantly reduced timing jitter. The camera also operates using a Gig-E interface (capable of transferring data up to 1GB/s) and thus can frame at over 30 fps streaming data directly to a hard drive. The stability of the external triggering of the new cameras was conducted using three camera systems triggering from the same source. The results indicate that the timing jitter was less than 20 ns. Calibrating a porous polymer PSP using the three cameras show essentially no change in the paint performance. These cameras were used for the second tunnel entry.

Due to the testing and safety requirements as well as efficiency, it was necessary to have nearly full remote control of the pan and tilt as well as focus of the cameras during the test. The cameras were mounted onto a commercial pan/tilt head that was capable of being controlled at distances of several hundred feet. Remote focus and zoom lenses were also employed to remotely focus the cameras.

Data Acquisition

All image acquisition was accomplished using the lifetime-based approach, which was found to be essential in previous testing.[5-6] However, these previous tests employed LED-based arrays and functioned by on-chip accumulation of several images to build the necessary data. This was shown to suffer from excessive blurring due to flapping and lead lag of the blade. Thus, a method to acquire the data in one single rotation was needed to account for this. Using the high powered pulse laser provided sufficient
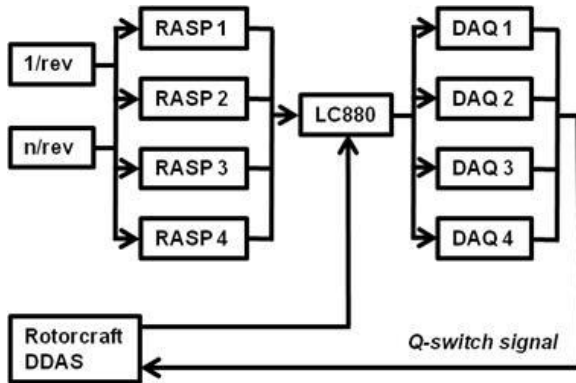
Figure 7. Timing schematic for multiple laser/camera systems (though only two were used in this test). LC880: Programmable logic gate controller; DAQ: Laser/camera system; DDAS: Dynamic Data Acquisition System.
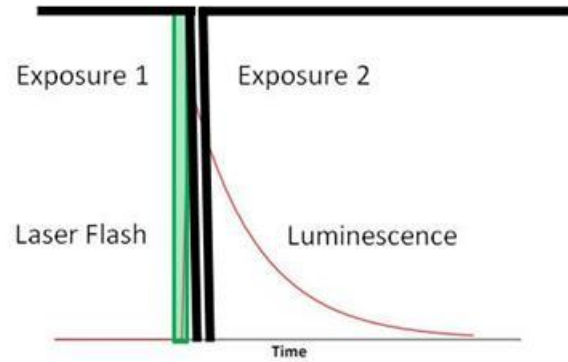
Figure 8. Schematic representation of data acquisition using dual frame imaging and laser pulse excitation. Laser pulse width and delay between images is exaggerated to show difference

levels of illumination and operating the cameras in the double exposure mode described above allowed the acquisition of the two gate images from one laser pulse. In addition, there was a requirement to synchronize the actual PSP data acquisition with the wind tunnel dynamic data acquisition system to be able to compare the dynamic pressure transducer measurements with the PSP at the correct azimuth positions. Timing for the acquisition was accomplished using a custom designed and built system based on a configurable counting board and software interface (Rotor Azimuth Synchronization Program, or RASP[26]) and the signals from the 1/ref and 1024/rev encoders on the GRMS. The RASP allowed for accurate and reproducible alignment of the blades with a specific azimuth location in the rotor disk. Programmable delay generators were also used to synch the camera acquisition with the flash lamp and Q-switch firing of each laser head. The overall control of the data acquisition was accomplished via an external signal sent from the wind tunnel dynamic data acquisition system. Each individual firing of the Q-switch was also recorded by the dynamic data acquisition system to enable comparison between the pressure transducer data with the PSP data at the same rotor azimuth. A simplified diagram of the timing setup is shown in Fig. 7.

The actual acquisition of the PSP data was acquired using a double frame imaging technique in which a short exposure image was taken followed immediately by a longer exposure image, as described by Juliano *et al.*[21] The longer exposure image was started after the interline transfer time of the pixels (200 ns) and lasted as long as it took for the first image to be read into the on-board RAM of the camera (for the PCO1600) or downloaded to the PC (for the cameras developed for the second test entry). For an image pair, the camera was set for an initial exposure time corresponding to the optimal delay between flash lamp and Q-switch firing. The initiation of the camera exposure also triggered the programmable delay generator to trigger the flash lamp and Q-switch at the desired times. These times were set to ensure that the laser flash occurred just before the end of the first exposure, exciting the paint. Then the second image was collected so that the remainder of the excited state decay occurred in this frame. A diagram of the nominal PSP imaging process is shown in Fig. 8.

For the first test entry, PSP images were acquired on the ABS at an approximate rotor azimuth of 98 degrees and on the RBS at an approximate rotor azimuth of 258 degrees. The ABS is the side where the blade is advancing into the freestream velocity and the RBS is the side where the blade is moving in the same direction as the freestream. For the second test entry, the ABS camera was moved to an azimuth

10

location of 0 degrees (over the tail) to investigate possible rotor-tail interactions. All data were acquired from the same blade and rotation speed was 1150 rpm.

Data Analysis

Data analysis for this work followed the standard procedure for analysis of PSP data acquired using the lifetime-based data acquisition procedures with some exceptions. Usually the lifetime-based data analysis is simply dividing Gate 1 by Gate 2 to form an I_{REF}/I image. However, the chosen paint formulation (the porous polymer) displays a significant change in performance that is tied to the application process. This phenomenon has been observed previously in many PSP formulations[27-29] but is very pronounced in this formulation. Essentially, the excited state lifetime of the Pt(TfPP) shows heterogeneity with application, where the lifetime can change dramatically based on the relative localized concentration of the probe. To solve this, a single wind-off image set was acquired immediately after the overspray. Since the overspray was done each morning, this wind-off image set was also acquired each morning. The wind-off image pair served as a further reference for the lifetime data and can account for much of the non-homogeneity effects. The basic data analysis used the following protocol:

1. Background correction of all images and deblurring of appropriate images

2. Registration of wind-on images Gate 1 and Gate 2 to the second gate image of the wind-off pair

3. Creating a "ratio of ratios" image using the wind-off image pair

4. Mapping the resultant image to the surface grid using the previously determined three dimensional coordinates of registration marks added to the blade

5. Final calibration of the image to convert to pressure. This was accomplished using hybrid calibration[9] by performing an *a priori* calibration using Eq. (3) and correcting any bias error using the pressure transducers.

However, for the second entry in which the entire upper surface is imaged, there was a serious mismatch of the wind-off images from the wind-on images. Thus, most of the data analysis needs to be performed on the surface mesh of the blade. For this entry, the following protocol was employed:
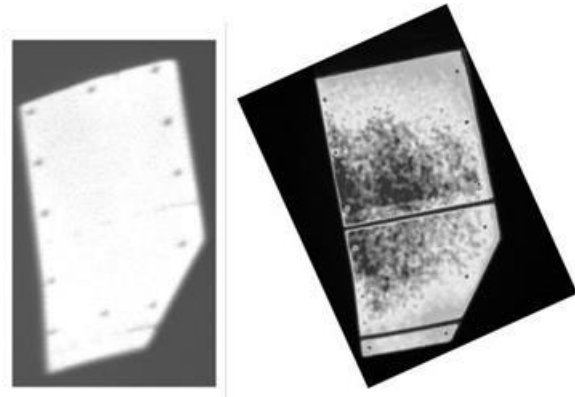
1. Background correction of all images

2. Registration of wind-on images to the Gate 1 of the first wind-on pair collected

3. Registration of wind-off images to the Gate 1 of the first wind-off pair collected

4. Creating a wind-on ratio and a wind-off ratio

5. Mapping the resultant images to the surface grid using the previously determined three dimensional coordinates of registration marks added to the blade

6. Creating a "ratio of ratios" on the mesh using the wind-off images

7. Final calibration of the image to convert to pressure.

11

Results and Discussion

Improvements from Using Laser-Based Data Acquisition

An initial concern with using a pulsed laser for illumination was the pulse-to-pulse repeatability of the laser itself. For the lasers used in this test, the stated power stability is +/- 4%, which could results in pressures errors up to 6%. However, since all data is taken in a single laser pulse through the interline transfer technique, the variation of the laser pulse power is not a concern. The benefits from using the laser-based data acquisition technique were apparent from the start. The greatest improvement was the clarity of the images. This is depicted in Fig. 9, which shows a comparison of a raw image taken using the LEDs and integrating over multiple revolutions and a raw image from this test. Because of the multiple revolutions that were required for the LED-based approach, the image has noticeable blur around the pressure transducers, especially when compared with the laser-based data acquisition technique. While the laser-based acquisition technique significantly reduces the blur caused by acquiring data over multiple rotations, it cannot compensate for rotational blur. The rotational blur is due to the exposure time of the second gate image and the motion of the blade. The second image is acquired

Figure 9. Raw images from LED-based (left) and laser-based (right) data acquisition techniques showing the reduced blurring.

after the laser pulse and is effectively the length of the luminescent decay, on the order of 5-10 microseconds (for this formulation). Thus, the exposure time of the second image is two to three orders of magnitude longer than the exposure time of the first image (the exposure time of the first image is governed by the laser pulse, which is ~ 10 ns wide). As a result of this, there is a rotational blur imparted to the Gate 2 image which is most evident at the trailing and leading edges, though does have an effect across the surface as well.

Juliano, *et al.*,[30] have developed a method to deconvolute this type of blurring from an image by using a Point Spread Function (PSF) for the blur. Construction of the PSF for the blurred rotor blade was constructed by first assuming the luminescent intensity decay was first order

$$I = I_0 * e^{-t/\tau} \tag{5}$$

where I is the intensity, I_0 is the initial intensity at the excitation peak, t is time, and τ is the excited state lifetime of the luminescent material. The blade rotates as a solid body, wherein the distance moved (Δx) at a point is proportional to the angular velocity, ω, and its radius from the center r ($\Delta x = \omega r \Delta t$). The motion was treated as rectilinear: the angle moved by the blade during 10τ was only 0.01 radian (less than $1°$), so the width of the path traced by a point on the blade was sub-pixel (but about 20 pixels long at the tip). By combining I(t) and Δx(t), the PSF can be defined as

$$I = I_0 * e^{-\Delta x/(\omega r \tau)} \tag{6}$$

12

Application of this PSF to the second image greatly reduced the blur as seen in Fig. 10. The effects of the deblurring algorithm on the recovered PSP results are shown in Fig. 11. Visual inspection of the images in Fig. 11 show that the most dramatic effect of the deblurring technique is on the trailing edge. This is also shown in the graph of Fig. 11, which is a comparison of a chord of PSP data. The deblurring technique greatly reduces the anomalous high pressure region at the trailing edge and shows little effect over the rest of the blade. However, in regions of sharp edges (such as the leading and trailing edges), this technique does introduce a slight ringing. All data analyzed from the first test entry (looking only at the tip) was deblurred using this technique.
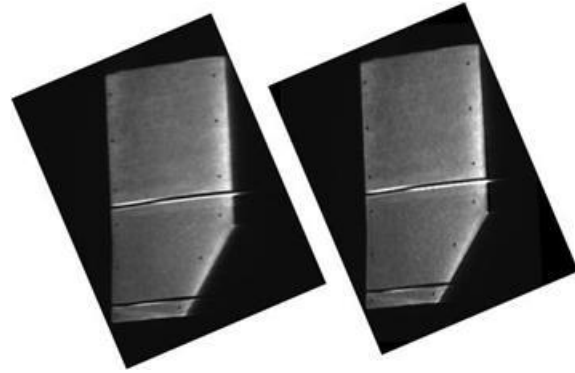
Figure 10. (Left) Original Gate 2 image showing the rotational blur. (Right) Same image after the deblurring technique described by Juliano, *et al.*

An additional benefit of the laser-based data acquisition is the greater increase in efficiency. Acquiring a data image over multiple revolutions required data acquisition times on the order a minute to acquire a single image pair. This precluded many of the advantages in signal-to-noise that can be achieved with averaging. Additionally, the comparison with pressure transducers would become tenuous as only an ensemble average could be used over that time frame, severely mitigating any dynamic effects that may exist. Alternatively, with the laser-based data acquisition technique, an image pair can be obtained in single laser flash, corresponding to a single rotation. Now, the comparison with pressure transducers is much cleaner as the image is collected at a single point in time. Also, with the current setup, as many as
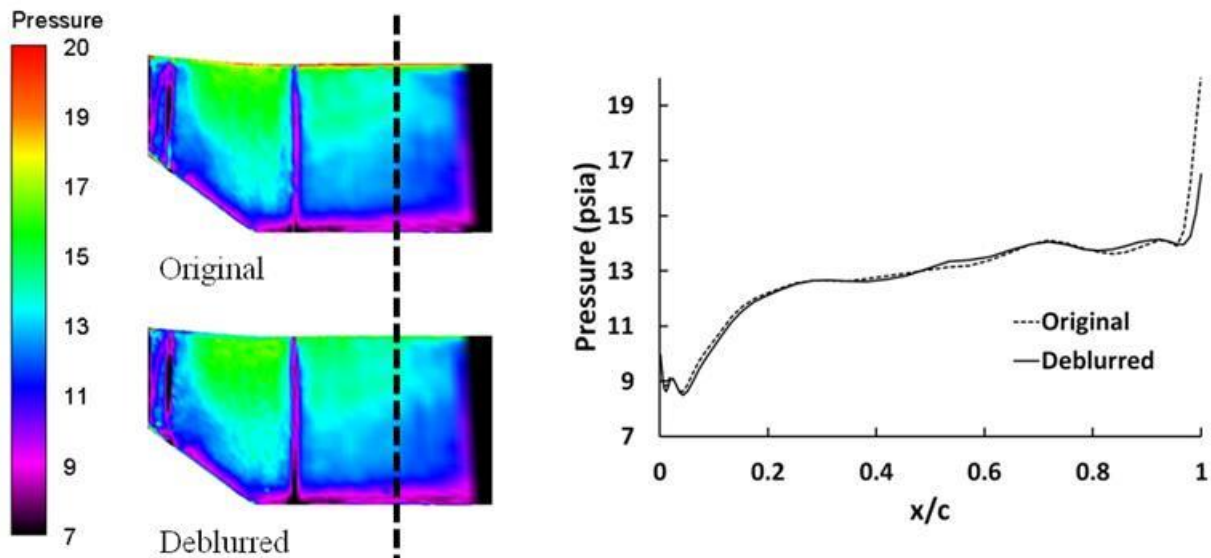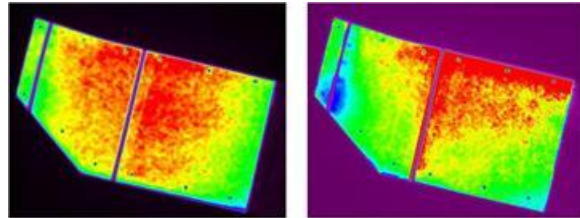

Figure 11. Comparison of PSP results obtained without (Original) and with (Deblurred) the application of the deblurring algorithm. The dashed line in the figures represents the location of the chord used for the comparison in the graph at the right.

30 image pairs could be obtained in a single test point collection from the rotorcraft dynamic data acquisition system, which required approximately 15 seconds.

Results from Test Entry 1

As mentioned in the Data Analysis section above, a single wind-off image pair was needed to correct some anomalies that happen with this particular paint formulation (the porous polymer PSP). In the wind-off image pair collected for this work, there was a series of anomalies that occurred near the pressure transducers. This is shown in Fig. 12. In the first gate image (left), the effect is not really noticeable. However, in the second gate image (right) there are significant variations at the transducer row at 99% chord. This image contains most of the excited state decay, thus any variations in the lifetime should be convoluted with the actual excitation field. After the test entry occurred and many discussions with the blade fabricators, it was postulated that these anomalies are due to the temperature compensating electronics of the Kulite sensors. This was a reasonable assumption as only the 99% chord pressure transducers were actually active for this test, and the anomalies are not seen at the 93% chord Kulites.

This effect was confirmed by imaging the blade with a thermal (IR) camera. This occurred after the test was complete and the Kulites in all of the blades were repaired. For this test, the blade was positioned on the bench top and the Kulites powered with 10V (as is done during normal operation). With the IR camera imaging the blade, the Kulite system was powered on.

Figure 12. Raw wind-off images. (Left) The first gate image taken at the laser flash; (B) the second gate image encompassing the majority of the excited-state decay showing the anomaly at the 99% chord transducer row.
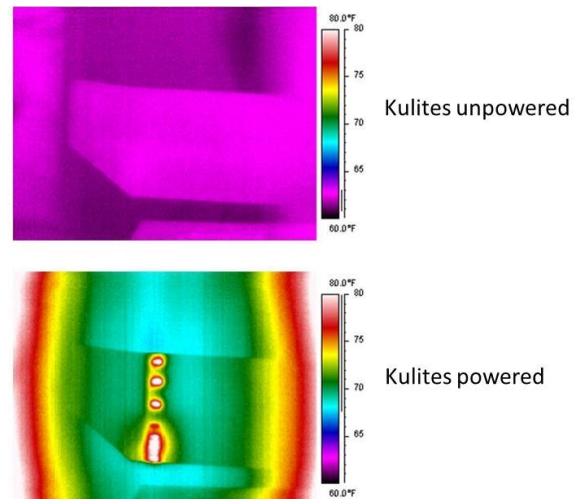
Figure 13. IR images of the blade before (Top) and after (Bottom) powering the Kulite transducers in the 93% chord row.

Within a very short time (a few seconds), the position of the Kulites became very noticeable in the IR image, and stabilized after a few minutes to show localized heating increases of ~10 $^{\circ}$C. Representative IR images before powering the Kulites and after is shown in Fig. 13. It should also be noted that this effect is only seen in the wind-off images. It can be assumed that in the wind-on condition, there is enough air flow to cause this heat to be convectively dissipated. For this entry, the Kulites were continuously powered to ensure that they had adequate temperature compensation. However, for future testing, a modification of this was put in place to allow for the remote depowering of the system to mitigate this effect.
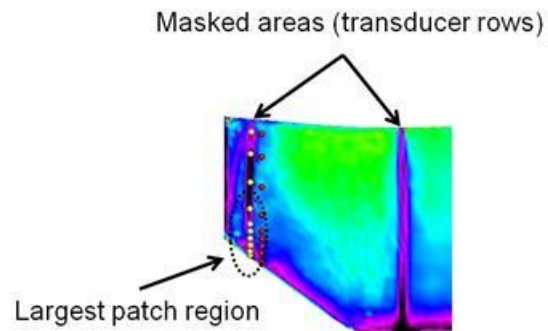
For this entry, however, a means to mitigate this was attempted by simply "cloning" this area of the paint with small regions near the 99% chord row. A comparison of the wind-off I_{REF}/I image before and after

the "patching" is shown in Fig. 14. Ideally, this image should have a uniform appearance, but lifetime variations in the paint (again, usually caused by application) can be seen. In the original image (left), these variations at the 99% chord are extreme. Patching (right) can remove much of this effect. Obviously this can bias the results in this region, so further study on the effects needs to be carried out as well as strategies to mitigate the effect from happening in the first place. All data analysis was accomplished using the patched reference images.
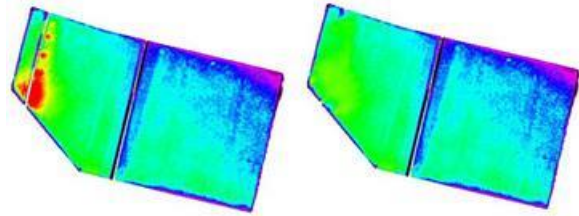
Figure 14. Wind-off Gate 1/Gate 2 images. (Left) Original images showing Kulite heating; (right) patched images showing nearly complete removal of the heating.

For the hybrid calibration mentioned in the Data Analysis section, the location of the pressure transducers was virtually moved on the surface grid away from the taped regions. If the pressure transducers would have been covered with only a small piece of tape individually, this probably would not have needed to be done. However, the tape strip afforded the maximum protection to the transducers, as well as significantly reduced the amount of time needed for application. For the final data analysis, the transducers were virtually moved toward the hub about 0.3 inches (0.5%R). This move was also structured to maintain the same locations in x/c as were in the original. This moved the transducers a significant (> 5 pixels) distance from the transducer to allow their use in calibration (the spatial resolution in the blade is ~0.03"/pixel)


Figure 15. Blade tip region detailing masked areas the original transducer locations (yellow spheres) and the transducer regions after moving inboard 0.3 inch (red spheres).

while keeping a close proximity to their actual location. All PSP comparison to the measured pressure from the transducers was carried out in this region. Unfortunately, the largest contamination region also corresponds to this region. However, due to the highly three-dimensional flow at the tip, it is not reasonable to move the virtual transducer line any further from the true transducer line. The effect of the Kapton tape as well as the original and virtually moved transducer locations are shown in Fig. 15.

With the transducers virtually moved to a clear region, they can now be used to anchor the *a priori* calibration, which was calculated using an assumed temperature. A comparison of the *a priori* calibration with the hybrid calibration is shown in Fig. 16. The comparison between the pressure transducer measurements and the PSP data is also included and shows that the hybrid calibration does bring the PSP data closer in line to the transducers. It should also be noted that the PSP data at the extremely low x/c locations is probably biased due to a combination of unaccounted for blurring and the need for patching due to the contamination. Because of the higher concentration of transducers in this region, the contamination region was much larger (as seen in Fig. 15) and this corresponds to the region of poor correlation between the PSP and the transducers. Even with this, the PSP shows relatively good agreement with the transducers. For consistency, all final calibrations were done using the hybrid calibration technique to anchor the *a priori* calibration.
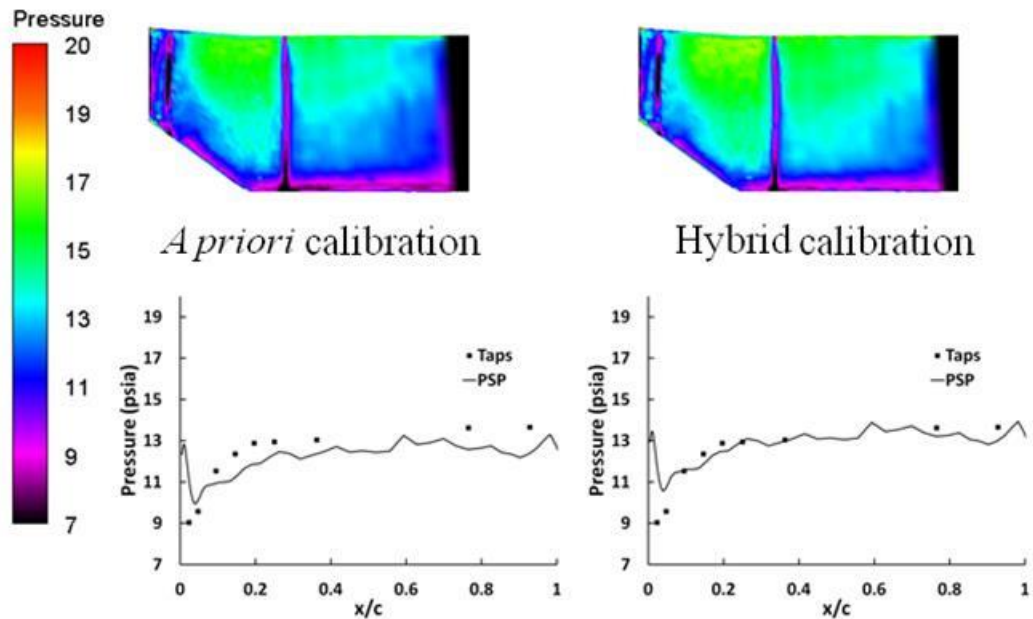
Figure 16. Comparison of PSP data calibrated using the *a priori* calibration (left) with an assumed temperature and the hybrid calibration (right) using the pressure transducers to "anchor" the *a priori* calibration. The comparison between the transducers and the PSP is shown below each image. The black region on the blade is unmapped data.

A representative set of data was acquired at a constant velocity of 138 knots (71.0 m/s) and at four thrust coefficients. A comparison of a PSP image at each thrust condition is shown in Fig. 17. This is the ABS and shows good qualitative agreement with what should be expected. It also shows that the pressure on
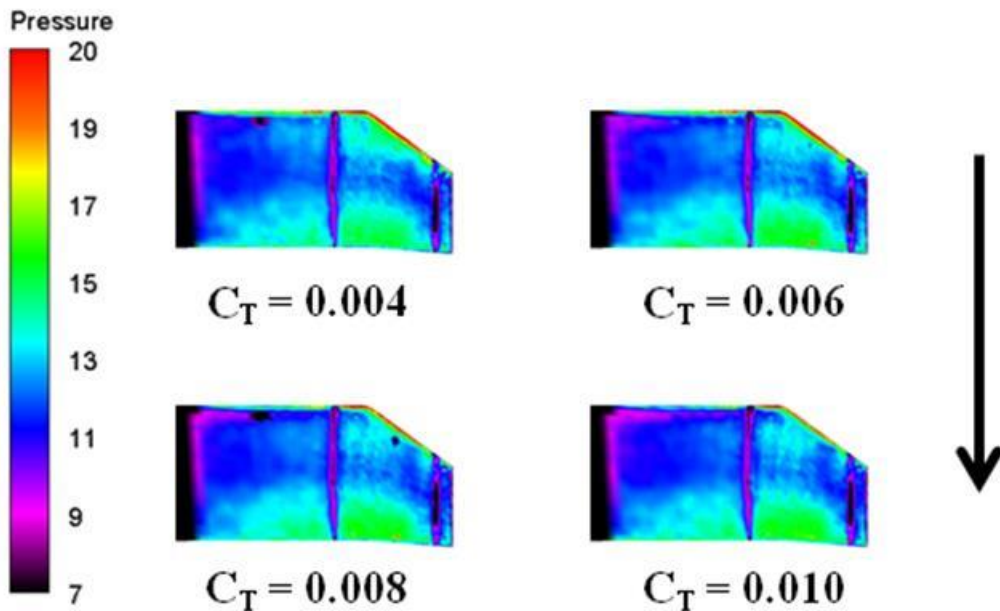
Figure 17. PSP images acquired from the ABS. The arrow represents the direction of the tunnel flow. The black regions on the blade are unmapped data.

the blade at this position has little dependence on the thrust coefficient. The comparison between the pressure transducers and the PSP is also shown in Fig. 18, and shows the same result. The PSP does not agree as well as the previous figure, most likely due to the smaller pressure changes on the blade as well as the reasons cited above (ringing from the deblurring technique as well as the patching used to account for the temperature effects from the Kulites in the wind-off image). However, both the PSP and the transducers show the higher pressure region at the extreme leading edge with the pressure decreasing as the flow accelerates over the center of the blade, followed by a gradual return to higher pressure at the trailing edge. As with the PSP data, the pressure transducer measurements also show little dependence on the thrust coefficient.

Figure 18. ABS comparisons between PSP data and pressure transducer measurements from Fig. 17.

The reason for the relatively small variations in pressure with C_T on the ABS is better illustrated by examining the ensemble averaged blade pitch during a revolution as shown in Fig. 19. The approximate locations of the measurement are shown by the dashed lines, with the ABS taken at $\Psi = 101^o$, the blade pitch for all of the cases is almost identical with only 0.6^o separating the $C_T = 0.004$ and $C_T = 0.010$ cases. Thus, the nearly constant pressure distribution regardless of C_T for the ABS is to be expected.
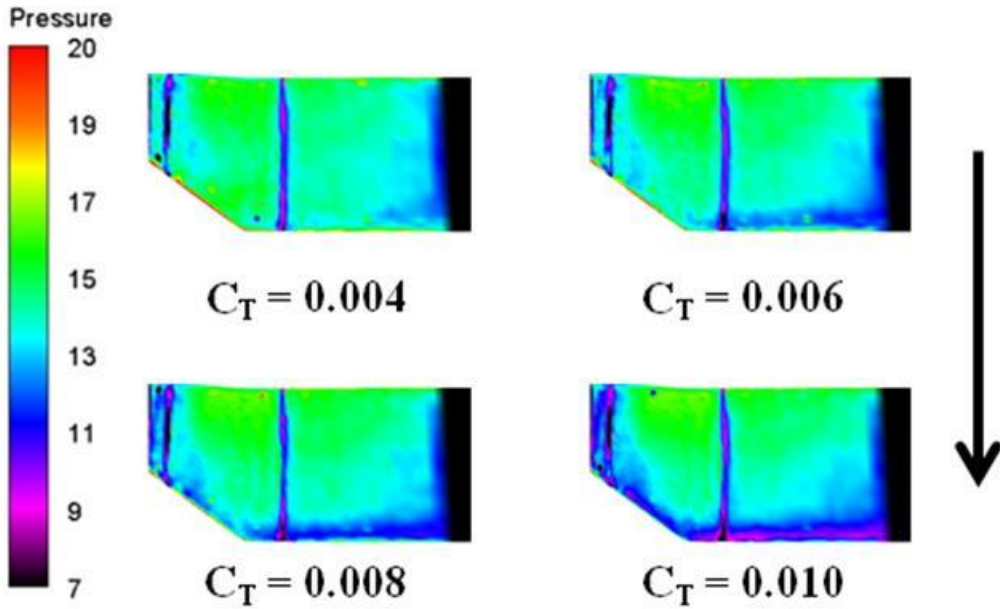
However, the same cannot be said of the blade in the "retreating" position (the blade

Figure 19. Average blade pitch during one revolution. The vertical dashed lines represent the azimuths where PSP data was collected.

is moving in the direction of the air flow in the tunnel). From Fig. 19 it is readily apparent that when $\Psi = 258^o$ (the measurement location for the RBS), the pitch angle increases approximately 12° through the thrust sweep. Thus, a much larger pressure dependence on C_T should be expected. Fig. 20 shows PSP data taken from this location. The PSP data shows that there is a much larger dependence on the thrust coefficient, as evidenced by the lower pressure region near the leading edge of the blade. Additionally, there is evidence of a flow phenomenon near the blade tip, such as a vortex shedding off the tip. This is highly dependent on the thrust coefficient, and evidence of it can be seen from C_T greater than 0.006. The larger pressure differentials are also evident from the pressure transducer and PSP comparisons, which is shown in Fig. 21. As with the previous data, the transducer agreement is very good (except near the leading edge). However, the flow phenomenon that is seen in the PSP at the tip does not appear in the transducer data. From visual inspection of the PSP data, it seems that the phenomenon flows just past the last pressure transducer, or possibly between two transducers. This does show one of the greatest

17

Figure 20. PSP images acquired from the RBS. The arrow represents the direction of the tunnel flow. The black regions on the blade are unmapped data.

advantages to using PSP: the ability to visualize and measure global pressure distributions as opposed to localized pressure measurements as is acquired from pressure transducers.

Results from Test Entry 2

For this test entry, the entire upper surface of the blade was painted. In addition, since there was little change in the measured pressures on the blade at the ABS, the imaging systems were moved to investigate the blade behavior over the tail. To fully image the upper surface of the blades, the imaging system was further expanded to include multiple cameras with overlapping fields of view. For the condition where the blade is over the RBS, three cameras were used; while two cameras were used to image the blade over the tail (technical limitations prevented the use of the third camera over the tail. The approximate fields of view of the three cameras over the RBS along with representative raw images are shown in Fig. 22.
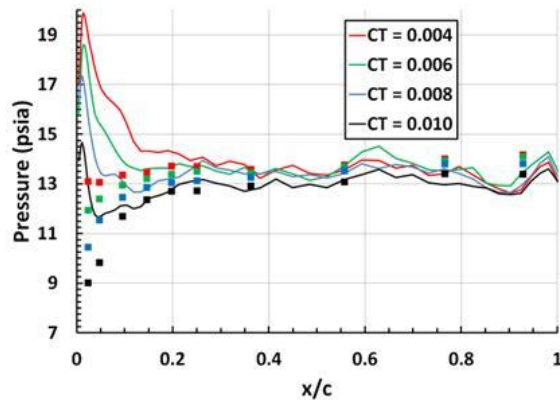
Figure 21. RBS comparisons between PSP data and pressure transducer measurements from Fig. 20.
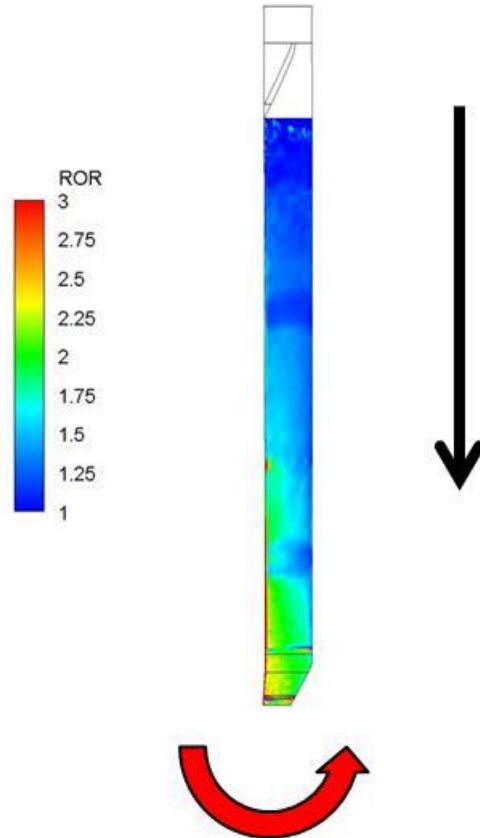
18
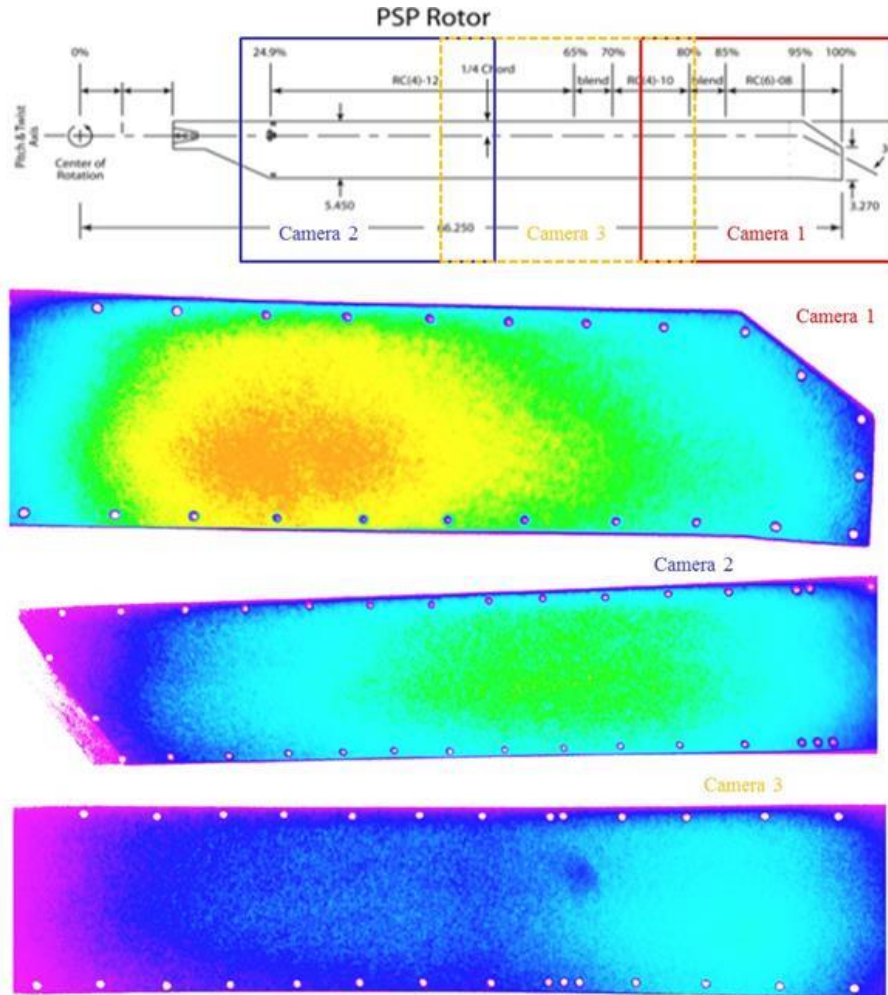
Figure 22. Approximate fields of view of the three cameras imaging the blade at the RBS as well as representative images.

This entry posed several new challenges. There was significant movement between the wind-off images and the wind-on images, requiring all of the data be processed on the surface mesh. A typical "ratio of ratios" image (wind-on image pair divided by the wind-off image pair) on the mesh is shown in Fig. 23. This image shows several aspects that need to be taken into account when performing these types of measurements. First, there is some slight misalignment between the wind-off and wind-on images, even when mapped to the mesh as evidenced by the slight misalignment of the pressure transducer rows at 99% and 93% chord. This is most likely due to the aeroelastic deformation that occurs, especially at the tip. This data is mapped to the *unwarped* mesh, even though under bending and twist, the blade does not have that same shape any longer. Second, there is an anomaly that can be seen at the trailing edge, which is most likely due to unaccounted for blurring in the wind-on image. The numerical deblurring technique described above would not completely remove this artifact with the addition of ringing noise due to the sharp intensity gradient present at these locations.[30] Third, there is a greater amount of overall noise present near the root of the blade. This is due to overall errors in the mapping of the data to the mesh. The coefficients for mapping the data were generated using reference marks (the transducers themselves) that

are clustered nearest the blade tip. For this model, there were no well-known reference marks near the root of the blade. Thus the coefficients for mapping needed to be extrapolated for these regions, leading to greater mapping errors. These errors tended to increase further away from the blade tip. Finally, there is a significant gradient along the span of the blade from the root to the tip. This is almost entirely due to the surface temperature on the blade itself. As mentioned previously, temperature is the major source of error in PSP measurements, and this is especially true in rotating environments where portions of the model can be rotating significantly slower than other portions. The rotation adds heat through simple friction, with the faster rotation generating higher temperatures. In the previous test entry, this effect was minimized as only the tip area was being investigated. However, when measuring over a large area as in this entry, temperature effects on the entire surface must be corrected.

As mentioned in the experimental two methods for accounting for blade temperature were attempted. First, a second blade was painted with a TSP and measured in close temporal proximity to the PSP blades. Second, three TSP "stripes" were applied to the PSP blade in radial locations as shown in Fig. 24. Since the excited state lifetime of the ruthenium complex was of the same magnitude as the Pt(TfPP), the same camera and laser timing could be employed for both paints.


Figure 23. Representative ratio-of-ratio PSP image. The red arrow represents the direction of blade rotation and the black arrow represents tunnel flow. Tunnel velocity is 120 knots and blade thrust (CT) is 0.08.

The results from the TSP blade at the same condition above are shown in Fig. 25. As should be expected, there is a significant temperature gradient (~20 $^{\circ}$C) along the span of the blade. However, there is also a chordwise temperature gradient which is rather surprising. While mapping the data to the surface mesh is crucial to adequately analyze the data, this process tends to smooth the data somewhat (as the mesh has much lower spatial resolution that the cameras). A TSP ratio image of the area near the root of the blade is shown in Fig. 26. This image is before mapping to the surface mesh, thus has the full resolution of the camera. From this data it is readily apparent that there are regions of significant temperature difference on the blade which tends to indicate that there is internal structure in the blade itself (e.g. a spar) that exhibits different thermal conductivity. The spar in question can be seen as a horizontal line in the image. The vertical lines are an artifact of the camera. In theory, if the blades are all made the same (which in this case is true), then this internal structure should affect the blades nearly equally, thus using the TSP blade, one should be able to account for the temperature effects on the PSP.
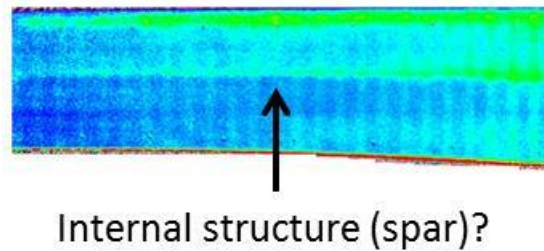
Figure 24. Locations of the TSP stripes applied to the PSP blade.
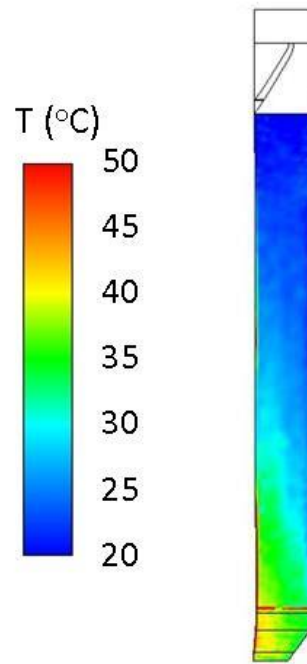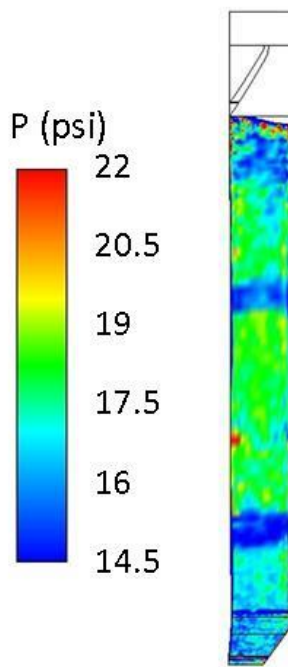

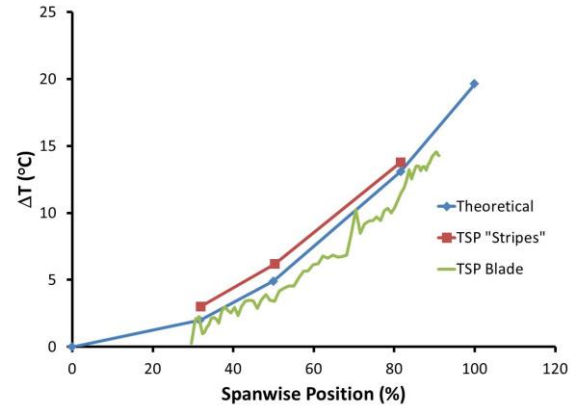**Figure 25.** Temperature measured by TSP blade. Conditions are the same as Fig. 23.

This was done by simply applying the calibration equation (Eq. 2) using a point-by-point temperature value calculated from the TSP. The results for this calibration are shown in Fig. 27, which show very poor results, with excessive noise as well as an overall offset to the data. The noise is most likely due to the fact that the TSP data was in fact acquired from another blade. The surface mesh that was used for this work was generated from a laser scan of the blade that was used for the PSP measurements. A separate surface grid for the TSP blade was not available, thus if there are slight differences between the two blades, this type of mis-alignment noise will manifest. In addition, the mapping coefficients for the TSP images were acquired using a similar procedure as the PSP images described above. However, in the case of this blade, there were even less reference markers (only one transducer row) that required using even

Figure 26. TSP ratio before mapping to surface mesh.

less reliable reference markers/regions (like blade tip, screw holes, etc.) that had even higher uncertainty. Thus, the mapping uncertainty for this blade is also higher. For this reason, temperature corrections must be carried out using the TSP "stripes" on the PSP blade.

Figure 27. PSP measurements corrected using temperature from TSP blade. Conditions are the same as Fig. 23.
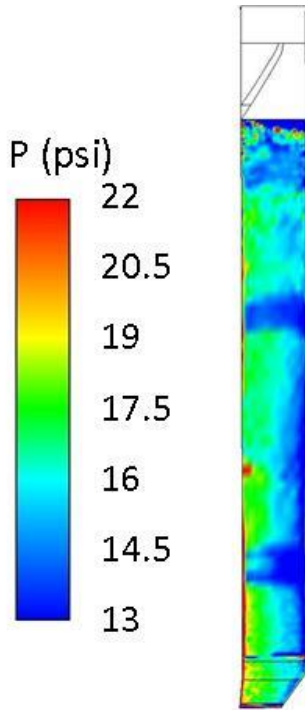

Figure 28. Comparison of theoretical blade temperature with temperatures measured by TSP stripes and TSP blade. Conditions are the same as Fig. 23.

The most likely theoretical temperature across the blade surface can be computed based on the local stagnation temperature. The temperature distribution should be parabolic as the local velocity of the blade is a function of radius, and therefore, the stagnation temperature will depend on the square of the radius. A comparison of these measured temperatures along a spanwise distribution and 50% chord is shown in Fig. 28. For **this case**, both the TSP blade and the TSP stripes follow the expected behavior qualitatively, though there is a deviation both from each other as well as from the theoretical value. The deviation between the TSP blade and stripe is most likely due to the difference in time between when each was collected. This would be expected and would also differ from run to run. The deviation from the theoretical temperature could be due to some thermal properties of the paint as well as the chordwise effects on the temperature distribution as shown in Fig. 25. For the temperature compensation of the PSP, the TSP "stripes" were used and fit to a linear solution to generate a calibration curve. A linear model was chosen based on the number of stripes available for use. It is fully realized that this could over- or under-compensate for temperature, especially at the blade tip.
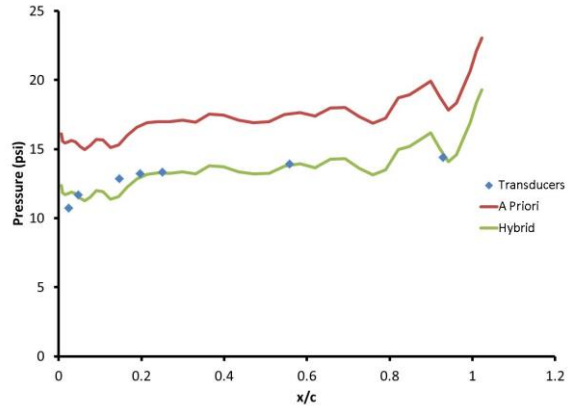
The results of this process are shown in Fig. 29. For this process, the linear regression of the TSP stripes was used to generate a pseudo-temperature image. Then this image is used to make a pixel-by-pixel correction of the PSP data using Eq. 2. While the results are much cleaner than those seen in Fig. 27, there still seems to be a bias in the data. This can be further seen if the calculated pressures are compared with the pressure transducers on the blade, as seen in Fig. 30. The *a priori* calibration shows a systematic bias from the transducer values. This is most likely due to uncorrected temperature, and could show a disadvantage of the method used to correct for temperature. However, if the hybrid calibration described in the previous section is used, the PSP shows good agreement with the transducers (except near the trailing edge, where the previous cited anomaly lies). When this calibration is applied over the entire surface of the blade, the results are shown in Fig. 31. However, some caution should be heeded when applying this type of calibration over an entire surface when only a few localized transducers are available
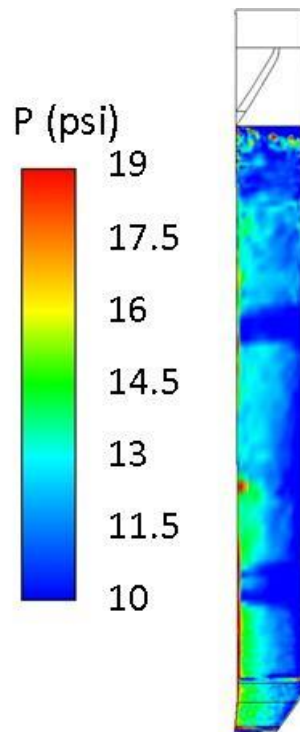
Figure 29. PSP measurements correct with the TSP slices. Conditions are the same as in Fig. 23.

Figure 30. Comparison of PSP data and transducer readings from Fig. 29. The red line is an *a priori* calibration of the PSP while the green line is a hybrid calibration of the PSP.

as this may bias other regions (e.g. near the blade root).

A sample of the results from a thrust sweep are shown in Fig. 32, For this data, the rotor speed and forward velocity of the wind tunnel were maintained at constant values. However, the lift was increased from $C_T = 0.04$ to $C_T = 0.094$. The results agree qualitatively with what should be expected (the lower pressure region at the leading edge of the blade becomes more pronounced at higher thrust conditions. These results show that reasonable PSP results can be obtained over the entire upper surface of the blade, though care must be taken to compensate for the natural temperature increase along the span of the blade.

Figure 31. PSP results obtained using a hybrid calibration. Conditions are the same as in Fig. 23.

23
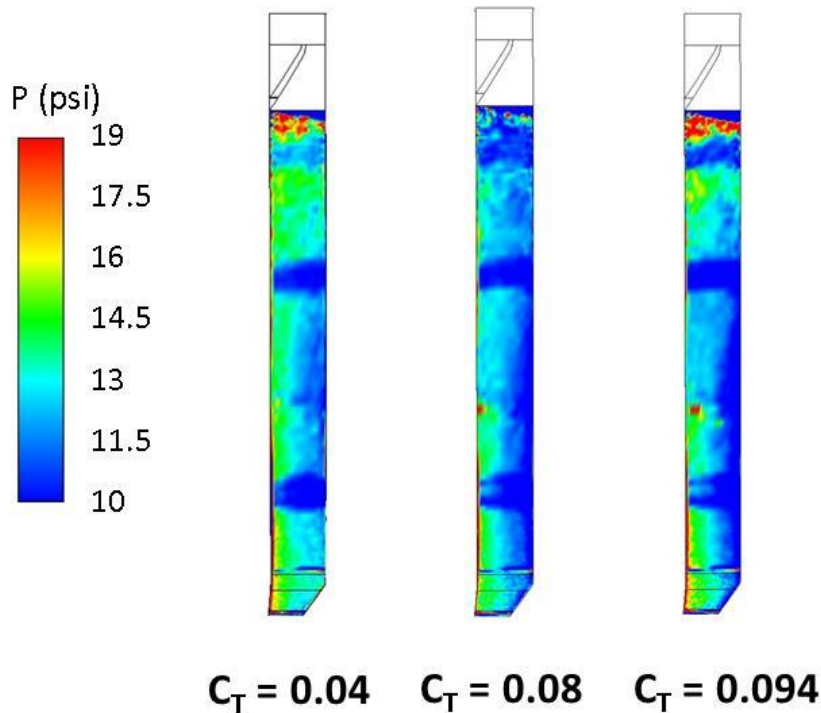
Figure 32. PSP results from a thrust sweep at the same conditions listed in Fig. 23.

Future Improvements

This work has proven that the PSP technique can indeed collect qualitative and quantitatively accurate pressure data from the surface of rotor blades in both hover and forward flight. However, there are several avenues which can be explored to greatly improve the efficiency as well as the results. Several have already been alluded to in this report, including better temperature compensation and the need to develop rapid shape determination procedures to be able to accurately analyze the data under aeroelastic effects. These efforts are currently underway, but there are other areas that also are being investigated and a summary of these follows.

### *Light shaping and steering*

Throughout both of these tests, several methods of trying to shape the light beam to concentrate the light into the areas of interest have been tested. One of the simplest ways was to simply insert a negative lens into the laser beam to spread the light into a spot. However, this lead to the creation of Newton rings through the lens that is then projected onto the surface. While the laser-based data acquisition technique is excellent for removing such laser phenomena as speckle as both images are acquired from the same laser shot, this is not the case with the Newton rings. When a pair of images that display these rings, ratioing them will still leave a significant interference pattern that is difficult to remove by compensation. In order to remove these rings, it was found that a diffuser was needed after the lens. The diffuser significantly destroyed the structure of the beam, thus removing the Newton rings. However, adding the diffuser caused an even greater expansion of the light, so that more than 90% of the light is being "thrown away" by illuminating everything except the blade. Several ideas for improving the spot generation are currently

Figure 33. Articulated laser arm.

being investigated. One of the most promising is to develop a parabolic reflector with a glass diffuser at the focus. The glass diffuser is strong enough to withstand the laser power, while the reflector can somewhat keep the scattered light from diffusing too much. The parabolic reflector can be machined in many different shapes (e.g. to produce an oval as opposed to round spot) and can be made to be mounted to a variety of components.

Another improvement with the laser spot is to include the ability to steer the beam. There are currently mechanisms capable of this, most notably an articulated laser guide. These are available from many different manufacturers and find common use in areas such as robotic laser welding systems. Several of these arms were used in the second entry test. However, without adequate control of the laser spot size, they were mostly just used to align the laser to the blade in a certain position and left stationary. One of these laser arms is shown in Fig. 33 attached to the mounting hardware used in the tunnel. If the development of the parabolic reflector is a success, then it is conceivable that this could then be attached to the end of the laser arm. Additionally, the end of the arm can be easily attached to a standard pan/tilt stage allowing of remote steering of the beam. Fig. 34 shows this type of arrangement.
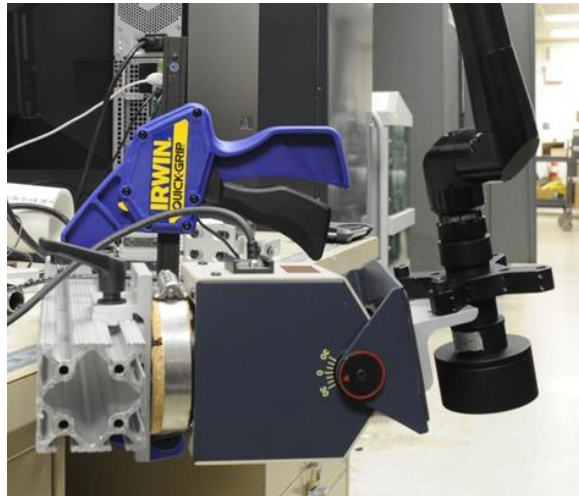
Figure 34. Articulated laser arm beam exit mounted to pan/tilt stage.

Remote Control of the Camera Field of View

For both entries described above, the cameras were placed on standard pan/tilt stages and used remote focus zoom lenses for increased efficiency as well as remote operation. The current system operates productively at a specific experimental condition. The implementation of the pan/tilt stages and remote focus/zoom/aperture lens means that if it is necessary to vary the field of view, this process can be accomplished without shutting down the tunnel. Unfortunately, the use of 6 cameras and 4 lasers means that the system requires 10 pan/tilt stages and 6 lens controllers. The system, as currently constructed, employs manual controllers for each lens and stage, and therefore, the process of modifying the field of view is quite slow. Furthermore, it is not possible to restore the system to a specific position for later testing.

There are several commercial systems available that are more rugged than the one currently used. Stages such as PT-CP-S4 from Telemetrics include a stiffer motor, Ethernet communication, presets, and a lens controller all for about $15,000. While an interesting option, the device was designed for video surveillance and does have some limitations. There is not readily available software development kit for integration of the system into the data acquisition program and there is a limited selection of lenses. Other options include devices built for studio production film cameras. These are generally very expensive (starting at $40,000) and still lack some features that would be of value.

Ideally, a package designed specifically for a PSP system would be ideal. The specific requirements of a system likes this would include:

1) Integrated pan/tilt and remote focus/zoom/aperture

2) Stiff stages that can carry at least 5-kg loads

3) Ethernet control of all components over a single IP

4) Presets on all components

5) Compatibility with a variety of lenses

6) A programmable interface compatible with C or LabView or other language

A prototype of a device capable of this has been designed and constructed by Innovative Scientific Solutions, Inc. It was designed using servo motors manufactured for robotics and a custom built Ethernet based lens controller and the device is shown in Fig. 35. This is a motor-controlled pan and tilt (P/T) mount optimized for remote operation and ideally suited for light bench-top work up to wind tunnel camera surveillance and data collection. The mount can be moved 60° to the left or right of center (pan) and 180° vertical up to vertical down (tilt) and support loads of 7 kg. Mounting feet are included that can accommodate ¼-20 or M6 screws on optical breadboards with 25.4 mm on center spacing. The mount utilizes a microcontroller for motion control and control of the remote focus, zoom, and iris lenses.

Figure 35. Prototype pan/tilt stage.

The articulation of the mount and lens settings are controlled by an intuitive LabVIEW graphical user interface (GUI). The standard software allows for 10 presets for lens (zoom, focus, and iris) plus pan and tilt, with more presets possible as an option. The speed of each motion and lens control is adjusted within the GUI. The GUI recognizes the device by its unique IP address. This allows networking of multiple P/T mounts via an Ethernet switch for multi-camera applications.
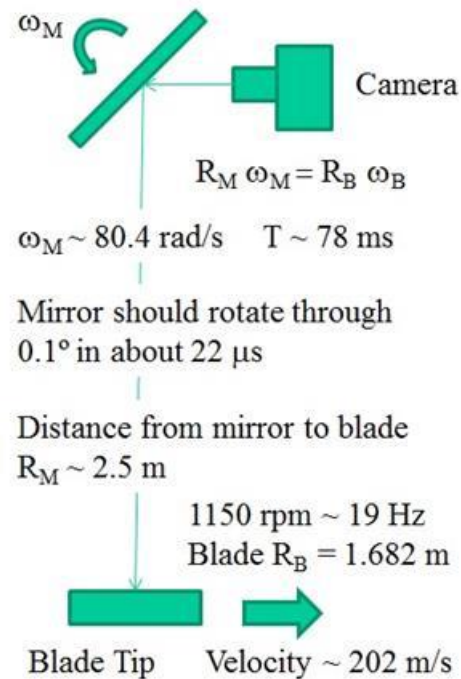
Motion Blur at Blade Tip

A numerical method to account for the motion blur exhibited in the higher exposure time second gate image was discussed previously, and used satisfactorily for some of the data. However, it does exhibit some limitations that were discussed previously. Ideally, a physical means to compensate for this type of blurring should be used. One method for optically correcting the motion of the blade is to use a mirror setup as shown in Fig. 36. The camera and lens are connected to a custom 2-inch galvanic mirror. The system is oriented so that the axis of rotation of the mirror is in line with the blade rotation. As the blade tip velocity and operating distance of the mirror are known, the rotation rate of the mirror can be estimated. For the tunnel entries described above, the operating distance is about 2.5 meters and the blade tip speed is about 200-m/s. A slew rate of about 80 radians per second is required for the mirror to track the blade. The custom galvanic mirror can be run from a simple ramp generator which is triggered externally, and therefore, blade synchronization is relatively simple. The resulting image should have very little motion blur, and therefore, the data at the leading and trailing edges should be improved.
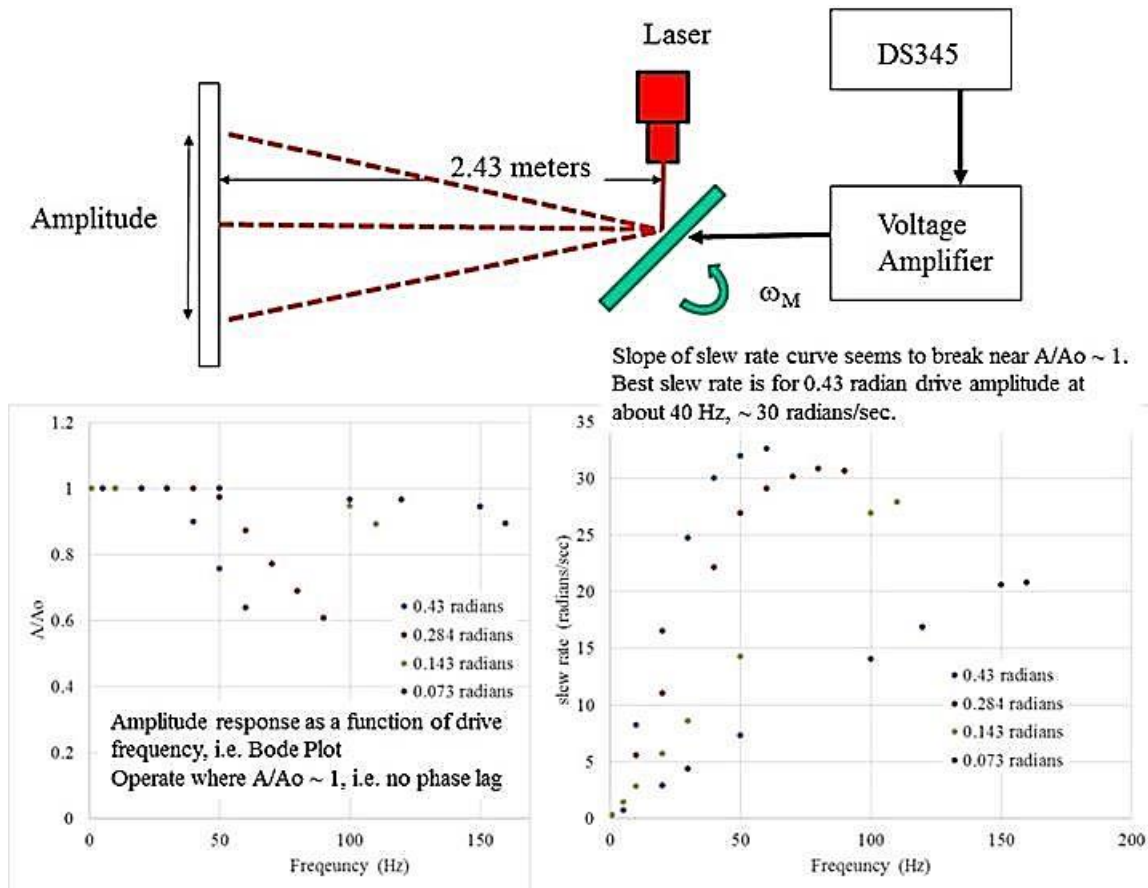
The galvanic mirror system is composed on a 2 inch mirror, a high voltage amplifier, and a Stanford Research DS345 Waveform Generator as shown in Fig. 37. The waveform from the DS345 drives the high voltage amplifier, which in turn drives the galvanic mirror. The amplitude versus frequency performance of the mirror was characterized using a laser, a pair of photo-diodes, and an oscilloscope. The laser was projected off of the mirror and onto a screen approximately 2.43 meters away. The amplitude and frequency of a sinusoidal waveform were set using the DS345. The amplitude of the mirror sweep was varied from 0.43 to 0.07 radians and the frequency was varied from 1 – 200 Hz. The amplitude of the mirror sweep was monitored on the screen, and the approximate slew rate of the sweep near 0 degrees was monitored using the photo-diodes.

The amplitude of the mirror sweep at each frequency was normalized by the amplitude at 1-Hz and plotted versus frequency for each drive amplitude. The resulting Bode diagram is shown in the lower left corner of Fig. 37. Note that the higher the drive amplitude, the lower the frequency at which the curve begins to exhibit amplitude clipping. Operation of the mirror in the flat portion of the curve is preferable, thus avoiding any phase lag or amplitude clipping issues. This should also allow the user to predict the mirror rotation rate and position accurately.

ω_M

Camera

$R_M\,\omega_M = R_B\,\omega_B$

$\omega_M \sim 80.4$ rad/s $T \sim 78$ ms

Mirror should rotate through $0.1°$ in about 22 μs

Distance from mirror to blade $R_M \sim 2.5$ m

1150 rpm ~ 19 Hz
Blade $R_B = 1.682$ m

Blade Tip   Velocity ~ 202 m/s

Figure 36. Galvanic mirror

While the amplitude data was being collected, the

Figure 37. Characterization of the galvanic mirror response.

photo-diodes were used to experimentally measure the rotation rate (slew rate) of the mirror near 0 degrees. The photo-diodes were placed about 10-cm apart along the scan line of the laser and the time between the passage of the laser over the photo-diodes was measured using the oscilloscope. This data was used to compute the angular rate of rotation of the mirror. This data was plotted as a function of frequency for each drive amplitude in the lower right corner of Fig. 37. Note that each curve is relatively linear below the frequency at which amplitude clipping begins. It is also clear that the maximum slew rate is achieved with the highest drive amplitude. A slew rate of about 30 radians/second is achieved at 40 Hz with a rive amplitude of 0.43 radians.

To demonstrate the application of the single-shot lifetime PSP system for rotorcraft applications, a simple rotating airfoil setup (Fig. 38, lower right corner) was constructed using a model airplane propeller and electric motor. The tip speed of this 225-mm diameter blade is about 100-m/s. One blade was painted with PSP and the laser, and camera with galvanic mirror were placed approximately 12 feet from the rotor hub. At this distance the mirror scan should generate an effective slew rate of 110 m/s, and therefore, it should be possible to compensate for the motion of the blade tip.

The rotor and mirror were first set to an off position, a data set was collected, and the Gate 2 over Gate 1 ratio was computed. This ratio, shown in the upper left corner of Fig. 38, displays no motion blur. The leading and trailing edge are well defined and there are no strong intensity modulations. The rotor was
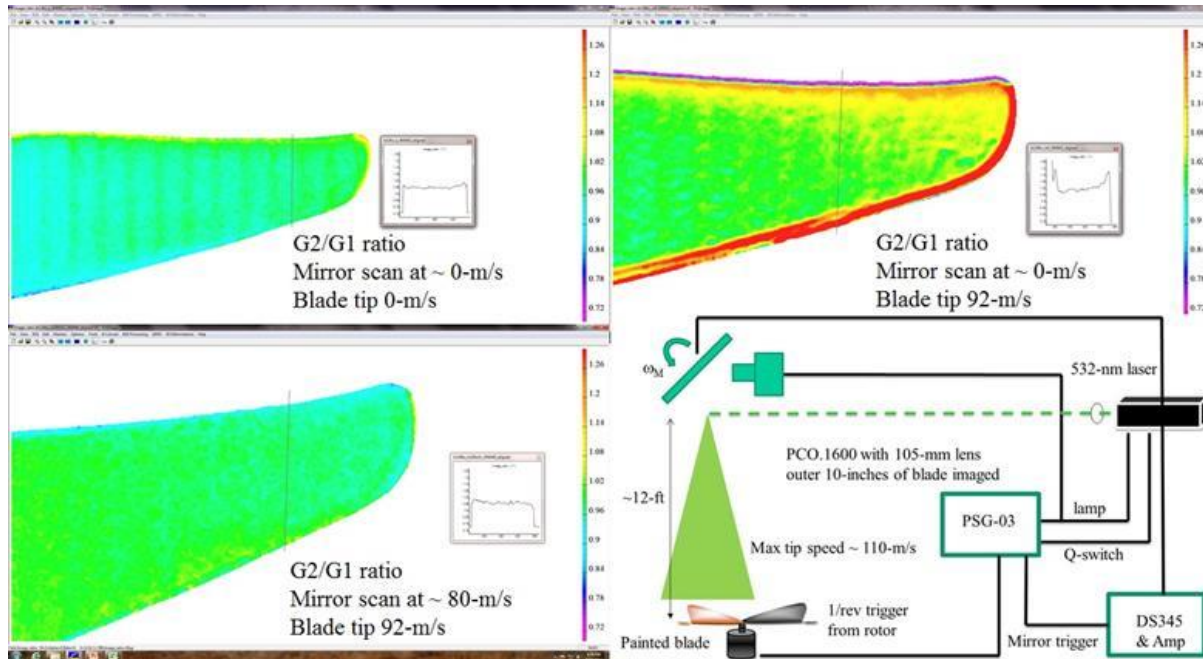
Figure 38. Use of galvanic mirror on airplane propeller.

then set so that the blade tip was at 92-m/s and the mirror was left stationary while a second data set was collected. This data set, shown in the upper right corner of Fig. 38, displays the motion blur issues. The intensity ratio is reasonable through the majority of the chord, but the leading and trailing edges show strong defects caused by the motion of the blade. Finally, the mirror was scanned and adjusted to a rate close to 90-m/s. Data was collected and the ratio of Gate 2 over Gate 1 is shown in the lower left corner of Fig. 38. Note the well-defined edges at the leading and trailing edges, similar to the stationary blade. This indicates that the galvanic mirror is effectively compensating for the motion of the blade.

A final demonstration of the galvanic mirror was also conducted in the second test entry. For this demonstration, the mirror was set to image the blade in the retreating position. The system was positioned about 30 deg. downstream of the RBS (so ~300°) and was triggered from the same system operating the RBS cameras. Timing for the mirror sweep involved acquiring the 1/rev signal from the rotor and using a delay generator to trigger the DS345 sweep. The mirror slew rate was set to its maximum value, which yielded an effective sweep rate of about 140-m/s.

Data was acquired at several test condition using the galvanic mirror. This data was acquired simultaneously with the retreating blade system, thus demonstrating integration of the galvanic mirror into the multi-camera system. An example of the Gate 2 image at the blade tip from the standard system and galvanic mirror system is shown in Fig. 39. It is noted that the galvanic mirror system position was not optimum as it was not directly over the blade and the slew rate was about 60% of the blade tip speed. The galvanic mirror position resulted in a lower signal level due to the longer operating distance and the use of a slower lens. The mirror system was successfully synchronized to the blade and image data was successfully captured with the existing PSP camera system.
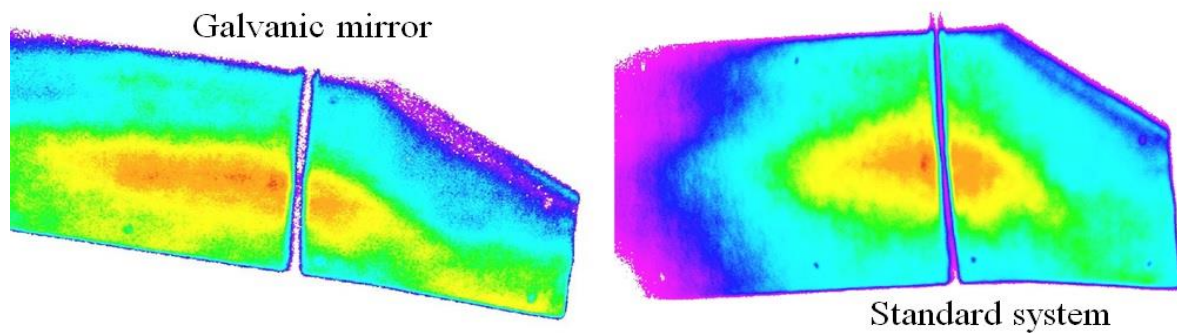
Figure 39. Gate 2 image of the blade tip with the standard system and galvanic mirror system.

Processing of Fast PSP Data

The single-shot data acquisition has matured over the last several years to a point where a substantial quantity of data can be acquired in a short time. The system demonstrated here composed of six 2-Megapixel cameras capable of streaming data over Gigabit Ethernet at over 10 fps. This can lead to a system capable of collecting hundreds of images at multiple locations in an azimuth sweep in a matter of a few minutes.

As an example, a 3 camera system placed over the retreating blade could collect 100 images at 2 degree increments over a +/- 10 degree blade sweep in under 5 minutes. This data set would include over 6000 images that must be processed. With the current data processing tools, this would require about 1 hour per image, or about 3 man years of labor. A reasonably productive day in the tunnel with a single 3 camera system is capable of producing more data than can be analyzed in a lifetime. Clearly, this issue must be addressed for the fast PSP system to be of value.

The current data processing method has been summarized previously. Resection markers on each image must be located manually prior to processing. The background is subtracted from each image and the ratio of Gate 2 over Gate 1 is computed for each image pair and any manual image processing to remove paint defects must be performed manually. The wind-off and wind-on ratio data must them be mapped to the mesh. Once on mesh, the ratio of the wind-off over wind-on is computed, a temperature correction is applied, any available pressure tap correction is applied, and the data is then combined with any overlapping camera views on the full mesh. This process must be repeated for all images at each station. It is also noted that the temperature correction can be quite complex on a rotorcraft flow due to the radial temperature gradient.

One means of quickly evaluating the data is to break the data set into mean and unsteady components. The mean pressure can be evaluated by aligning and averaging each Gate 1 and Gate 2 image from the full data set. These data are then processed using the wind-off image and the temperature correction. This data would represent the phase-averaged pressure on the blade at a particular station or condition. By averaging all wind-on images, the resulting data would have the added advantage of a good signal-to-noise ratio.

The unsteady pressure can be computed using only the wind-on data set. The averaged wind-on Gate 1 and Gate 2 data serve as the wind-off images, a running wind-off. The variation from this mean condition
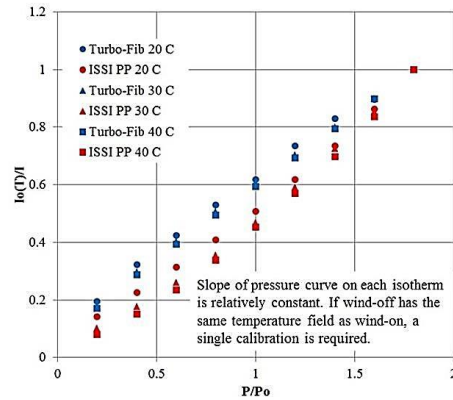
30

is computed for each image. This approach to processing the unsteady data has several advantages. These include processing all data on the bitmap, simplified mapping, and elimination of temperature errors.

Since all data was acquired at the wind-on condition, there is relatively little change in the image of the blade between the running wind-off and each wind-on image as is the case between the true wind-off and wind-on. This simplifies the mapping and allows the data to be processed on the bitmap. This also suggests that it may be possible to present preliminary data, such as RMS pressure fluctuations on the bitmap in near real time.

Figure 40. Calibration of porous polymer (ISSI PP) and Turbo-Fib (another fast PSP) showing ideal behavior.

A second advantage is that it is possible to process the unsteady data without knowledge of the local temperature distribution. The radial temperature gradient is already present in the running wind-off image. If one is using an ideal PSP with a linear slope, such at the PtTFPP-PP, this can be especially advantageous. An ideal PSP has the unique property of having a constant slope at a range of temperatures, as shown in Fig. 40. As the running wind-off and each wind-on image have the same thermal distribution, any temperature sensitivity is automatically eliminated from the unsteady data set and only the slope of the curve in Fig. 40 is required for converting the data to pressure.

This procedure was done for one of the camera views that encompass the data presented in Fig. 23 above. The first step in the process is to compute the average wind-on image for each gate. It is noted that there is some degree of jitter in the blade position from shot-to-shot, and therefore one cannot simply load and average the images without introducing a degree of smearing. A simple average of the data from Gate 1 is presented on the left of Fig. 41. Note that the edges of the blade are slightly blurred, and the markers are no longer distinguishable. The average image has been effectively low-pass filtered by the blade jitter.
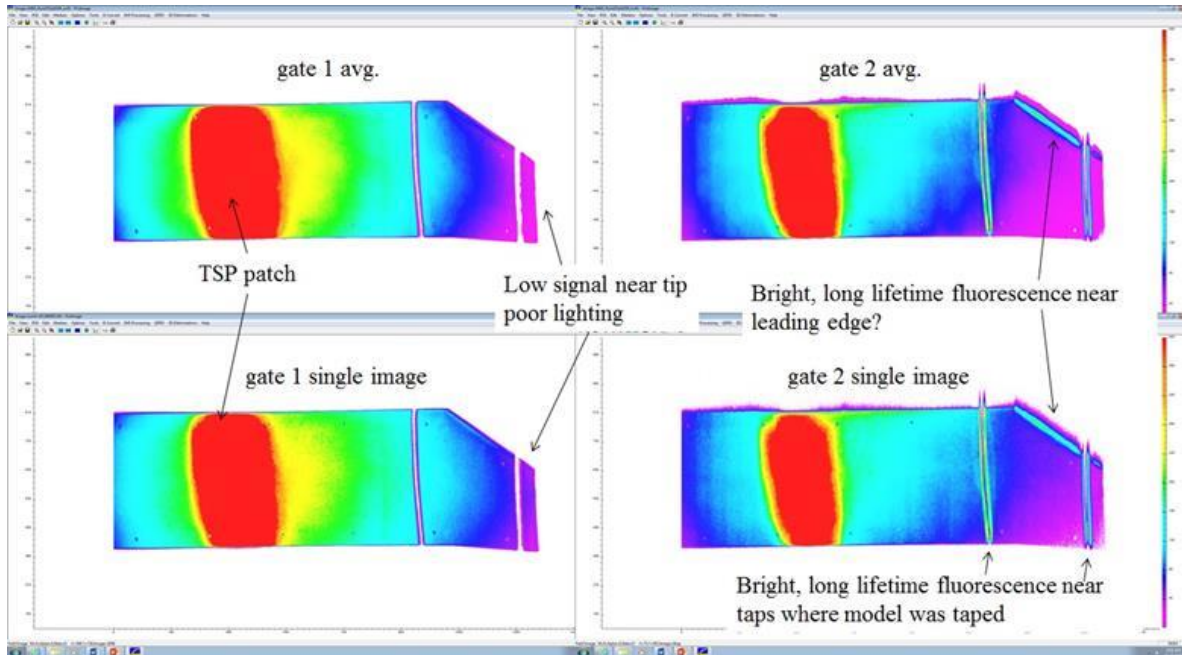
As described previously, it is possible to locate the markers on each image and map the data so that it would align, then average. The process of locating the markers and mapping each image is very time

**Figure 41.** Automatic image registration.

Figure 42. Registered and averaged images for the data set depicted in Fig. 23..

consuming, and this is just the kind of process that should be avoided for efficient processing of PSP data. An alternative solution was implemented using ImageJ.[31]

ImageJ is a Java based image processing package developed by NIH. A variety of user developed plug-ins can be downloaded, including an automatic image registration tool that operates on a stack of images. The image registration tool, StackReg,[32] operates by computing a cross-correlation between the images and performing a mapping, such as a translation or solid body rotation to the image. As the blades are solid bodies, a simple translation or solid body rotation is sufficient for the program to align all the images at a given test condition. The result of a StackReg and average is shown on the right of Fig. 41. Note that the markers are now distinct, indicating a successful alignment.

The data was registered and averaged using ImageJ. Once the images were aligned, the average Gate 1 and Gate 2 image were computed, these are shown on the left of Fig. 42. The registered stack of Gate 1 and Gate 2 images were then saved for processing, an example of an individual image pair is shown at the right of Fig. 42. Note that at this point, all images should be in alignment, thus greatly simplifying the conversion of the data to pressure. It should only be necessary to subtract backgrounds, ratio, and convert to relative pressure.

Close inspection of the images in Fig. 42 does reveal several issues. Of most concern is that the signal near the tip of the blade is quite low. This was a result of poor lighting near the tip rather than the paint signal. Means to improve this lighting have been discussed in the section above. A second issue is the presence of a long lifetime florescence at several points on the blade. Near the rows of pressure taps, the blade was taped before spraying to mask the taps. It appears that the overspray may have leached some material out of the tape adhesive and left a residue near the edges. This residue is fluorescent, and has a relatively long lifetime as all signal is present in Gate 2. This signal is most notable as streaks that appear

32
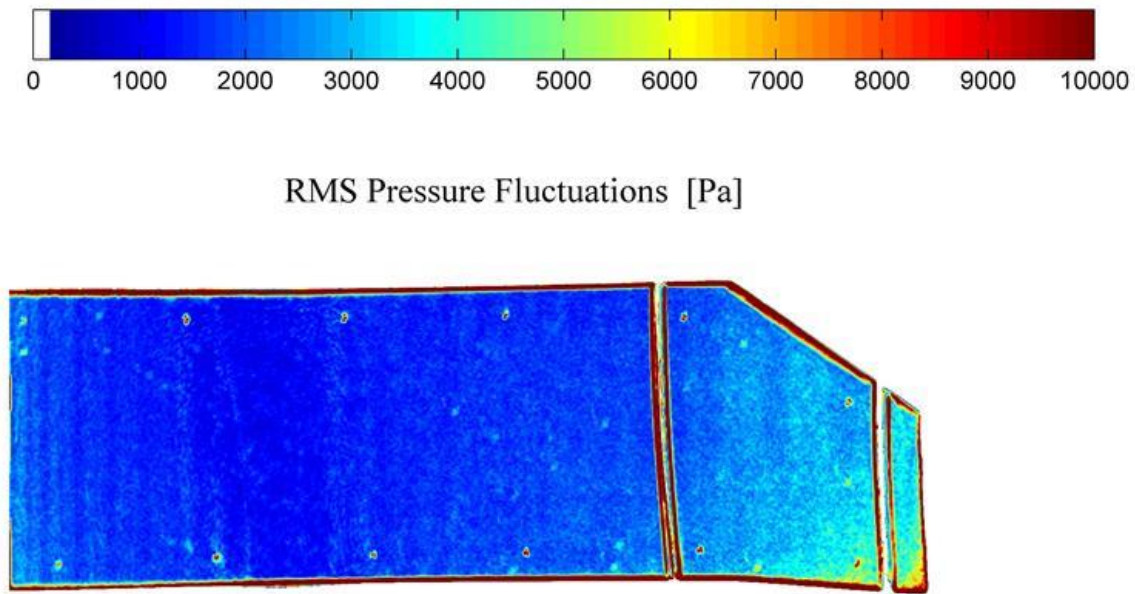
Figure 43. Image of RMS pressure fluctuations at the tip.

to lead the blade near the tap strips. It is also noted that a similar contaminate appears along the leading edge of the blade near the region of taper. No tape was used in this region, and therefore this is unexpected. The data in this region is likely compromised.

With the images aligned and the wind-on average computed, the data can be converted to pressure. A Matlab script was written that loads the images, applies a 5 pixel low-pass filter, computes the ratio, and converts the results to relative pressure. For this data set, 44 image pairs were processed and the RMS pressure fluctuation was computed. The script operated in about 5 seconds, demonstrating the potential for real time data visualization using this approach. The resulting image of pressure fluctuations is shown in Fig. 43.

Several comments regarding the data in Fig. 43 are relevant. The data indicate large amplitude of pressure fluctuations on the boundaries. This is likely an artifact of slightly misaligned images. The data also indicates a larger degree of unsteadiness at the tip, where the signal was low. To determine the validity of this data, it is necessary to estimate the uncertainty in the data.

For this estimation, we will consider the shot noise to be the dominate factor. The signal in Gate 2 was quite low in this data set, about 2000 photo-electrons over the main part of the blade and as low as 500 photo-electrons near the tip, and therefore, should dominate the shot noise. Assuming the use of a 5 pixel low pass filter, the shot noise from this tip region could be expected to be over 2400-Pa in amplitude. At most the amplitude of the pressure fluctuations are about 2-kPa on the main part of the blade and 5-kPa near the tip. Based on this rough estimation, it is likely that the pressure fluctuations shown in Fig. 43 are a result of poor signal-to-noise rather than real aerodynamic effects.

Conclusions

This study details a series of tests using PSP for the global pressure determination on the upper surface of rotorcraft blades in forward flight. These tests were performed using the General Rotor Model System installed in the 14- x 22-Foot Subsonic Tunnel at NASA Langley Research Center. Blades were painted with a porous polymer PSP formulation capable of routine frequency responses on the order of 5 kHz. The blades were instrumented with pressure transducers, with the actual blade used in the measurement instrumented with a row at 93% and 99% chord, respectively.

For this testing, a laser-based data acquisition system was designed and deployed. This system is capable of obtaining near instantaneous data by exciting the paint with the laser and using an interline transfer camera to take a pair of images. With correct timing, the laser flash occurs at the end of the first gate with the majority of the excited-state decay being recorded by the second gate. This is analogous to the traditional lifetime-based approach in which two images are collected, one during the excitation pulse, and one after the pulse.

Analysis of the data shows fairly good agreement (within 10%) of the pressure transducer measurements, though there are some issues that were encountered. First, care must be taken to ensure that the Kulite transducers are powered down for the wind-off images, as the temperature compensation of the transducers manifests as significant noise in the transducer area. Second, the rotational blur that is evident in the second image can limit the results, especially near the leading and trailing edges. A numerical method for compensating for this blur has been discussed and showed good results, though the edges are still suspect due to the addition of noise from the technique. Finally, if the entire upper surface of the blade is to be investigated, accounting for the temperature change across the blade is a must. Two methods for this were presented, and the best results occurred when TSP "striped" on the PSP blade were used for compensation.

Even with these limitations, the data agreed both qualitatively and somewhat quantitatively with the expected results. To date, these are some of the first successful tests of PSP on flexible rotating surfaces capable of measuring dynamic phenomena. Further enhancements in the instrumentation, data acquisition, and data analysis areas are being investigated.

References

[1]Lorber, P.F., Stauter, R.C., and Landgrebe, A.J., "A Comprehensive Hover Test of the Airloads and Airflow of an Extensively Instrumented Model Helicopter Rotor," *Proceedings of the 45th Annual Forum of the American Helicopter Society*, Boston, MA, May 1989.

[2]Lal, M.K., Liou, S.G., Pierce, G.A., and Komerath, N.M., "Measurements around a Rotor Blade Excited in Pitch, Part 2: Unsteady Surface Pressure," *Journal of the American Helicopter Society*, Vol. 39, No. 2, 1994, pp. 13-20.

[3]Gorton, S.A., Poling, D.R., and Dadone, L., "Laser Velocimetry and Blade Pressure Measurements of a Blade-Vortex Interaction," *Journal of the American Helicopter Society*, Vol. 40, No. 2, 1995, pp. 15-23.

[4]Lorber, P.F., "Aerodynamic Results of a Pressure-Instrumented Model Rotor Test at the DNW," *Proceedings of the 46th Annual Forum of the American Helicopter Society*, Washington, DC, May 1990.

[5]Wong, O.D, Watkins, A.N., and Ingram. J.L., "Pressure Sensitive Paint Measurements on 15% Scale Rotor Blades in Hover," *35th AIAA Fluid Dynamics Conference*, AIAA, Ontario, Canada, 2005, Paper 2005-5008.

[6]Watkins, A.N., Leighty, B.D., Lipford, W.E., Wong, O.D., Oglesby, D.M., and Ingram. J.L., "Development of a Pressure Sensitive Paint System for Measuring Global Surface Pressures on Rotorcraft Blades," *22nd International Congress on Instrumentation in Aerospace Simulation Facilities*, IEEE, Pacific Grove, CA, 2007, and published in the proceedings.

[7]Kavandi, J., Callis, J., Gouterman, M., Khalil, G., Wright, D., Green, E., Burns, D., and McLachlan, B., "Luminescent Barometry in Wind Tunnels," *Review of Scientific Instrumentation*, Vol. 61, No. 11, 1990, pp. 3340-3347.

[8]Morris, M.J., Benne, M.E., Crites, R.C., and Donovan, J.F., "Aerodynamic Measurements Based on Photoluminescence," *31st Aerospace Sciences Meeting*, AIAA, Reno, NV, 1993, Paper 93-0175.

[9]McLachlan, B., and Bell, J., "Pressure-Sensitive Paint in Aerodynamic Testing," *Experimental Thermal and Fluid Science*, Vol. 10, No. 4, 1995, pp. 470-485.

[10]Liu. T., Campbell, B., Burns, S., and Sullivan, J., "Temperature- and Pressure-Sensitive Luminescent Paints in Aerodynamics," *Applied Mechanics Reviews*, Vol. 50, No. 4, 1997, pp. 227-246.

[11]Liu, T., and Sullivan, J., *Pressure and Temperature Sensitive Paints (Experimental Fluid Dynamics)*, Springer-Verlag, Berlin, 2004.

[12]Lakowicz, J., *Principles of Fluorescence Spectroscopy*, 2nd ed., Kluwer Academic/Plenum Publishers, New York, 1999, pp. 239-242.

[13]Engler, R., and Klein, C., "DLR PSP System: Intensity and Lifetime Measurements," *17th International Congress on Instrumentation in Aerospace Simulation Facilities*, IEEE, Pacific Grove, CA, 1997, pp. 46-56.

[14]Holmes, J., "Analysis of Radiometric, Lifetime, and Fluorescent Imaging for Pressure Sensitive Paint," *Aeronautical Journal*, Vol. 102, No. 1014, 1998, pp. 189-194.

[15]Bell, J.H., Schairer, T.E., Hand, L.A., and Mehta, R.D., "Surface Pressure Measurements Using Luminescent Coatings," *Annual Review of Fluid Mechanics*, Vol. 33, 2001, pp. 115-206.

[16]Mitsuo, K., Egami, Y., Asai, K., Suzuki, H., and Mizushima, H., "Development of Lifetime Imaging System for Pressure-Sensitive Paint," *22nd AIAA Aerodynamic Measurement Technology and Ground Testing Conference*, AIAA, St. Louis, MO, 2002, Paper 2002-2909.

[17]Watkins, A.N., Jordan, J.D., Leighty, B.D., Ingram, J.L., and Oglesby, D.M., "Development of Next Generation Lifetime PSP Imaging Systems," *20th International Congress on Instrumentation in Aerospace Simulation Facilities*, IEEE, Gottingen, Germany, 2003, pp. 372-382.

[18]Gregory, J.W., Asai, K., Kameda, M., Liu, T., and Sullivan, J.P., "A Review of Pressure-Sensitive Paint for High-Speed and Unsteady Aerodynamics," *Proceedings of the Institution of Mechanical Engineers –*

Part G: Journal of Aerospace Engineering, Vol. 222, No. 2, pp. 249-290.

[19]Gregory, J.W., Sullivan, J.P., Raman G., and Raghu S., "Characterization of the Microfluidic Oscillator," *AIAA Journal*, Vol. 45, No. 3, 2007, pp. 568-576.

[20] Gregory J.W., "Porous Pressure-Sensitive Paint for Measurement of Unsteady Pressures in Turbomachinery," *42nd Aerospace Sciences Meeting*, AIAA, Reno, NV, 2004, Paper 2004-0294.

[21]Juliano, T.J., Kumar, P., Peng, D., Gregory, J.W., Crafton, J., and Fonov, S., "Single-Shot, Lifetime-Based Pressure-Sensitive Paint for Rotating Blades," *Measurement Science and Technology*, Vol. 22, No. 8, 2011, 085403 (10pp).

[22]Noonan, K.W., "Aerodynamic Characteristics of Two Rotorcraft Airfoils Designed for Application to the Inboard Region of a Main Rotor Blade," NASA-TP-3009, AVSCOM-TR-90-B-005, 1990.

[23]Noonan, K.W., "Aerodynamic Characteristics of Two Rotorcraft Airfoils Designed for the Tip Region of a Main Rotor Blade," NASA-TM-4264, AVSCOM-TR-91-B-003, 1991.

[24]Wong, O.D. and Watkins, A.N., "Blade Tip Pressure Measurements Using Pressure Sensitive Paint," *AHS International 68th Annual Forum*, AHS, Fort Worth, TX, 2012.

[25]Watkins, A.N., "Experimental Results for Temporally Overlapping Pulses From Quantel EverGreen 200 Laser," NASA/TM-2013-218057, 2013.

[26]Fleming, G. A., "RASP: Rotor Azimuth Synchronization Program (RASP) User's Guide, Version 1.3," NASA Langley Research Center, February 6, 2008

[27]Bell, J.H., "Accuracy Limitations of Lifetime-Based Pressure-Sensitive Paint (PSP) Measurements," *19th International Congress on Instrumentation in Aerospace Simulation Facilities*, IEEE, Cleveland, OH, 2001, pp. 5-16.

[28]Ruyten, W. and Sellers, M., "Lifetime Analysis of the Pressure-Sensitive Paint PtTFPP in FIB," *42nd Aerospace Sciences Meeting*, AIAA, Reno, NV, 2004, Paper 2004-881.

[29]Ruyten, W., Sellers, M.E., and Baker, W.M., "Spatially Nonuniform Self-Quenching of the Pressure-Sensitive Paint PtTFPP/FIB," *47th Aerospace Sciences Meeting*, AIAA, Orlando, FL, 2009, Paper 2009-1660.

[30]Juliano, T.J., Disotell, K.J, Gregory, J.W., Crafton, J., and Fonov, S., "Motion-Deblurred, Fast-Response Pressure-Sensitive Paint on a Rotor in Forward Flight," *Measurement Science and Technology*, Vol. 23, No. 4, 2012, 045303 (11pp).

[31]Available at http://rsb.info.nih.gov/ij/

[32]Available at http://bigwww.epfl.ch/thevenaz/stackreg/

REPORT DOCUMENTATION PAGE

Form Approved
OMB No. 0704-0188

1. REPORT DATE *(DD-MM-YYYY)*	2. REPORT TYPE	3. DATES COVERED *(From - To)*
01-05-2014	Technical Memorandum	

4. TITLE AND SUBTITLE

Applying Pressure Sensitive Paint Technology to Rotor Blades

5a. CONTRACT NUMBER

5b. GRANT NUMBER

5c. PROGRAM ELEMENT NUMBER

6. AUTHOR(S)

Watkins, Anthony N.; Leighty, Bradley D.; Lipford, William E.; Goodman, Kyle Z.; Crafton, Jim; Gregory, James W.

5d. PROJECT NUMBER

5e. TASK NUMBER

5f. WORK UNIT NUMBER

380046.02.07.03.03.01

7. PERFORMING ORGANIZATION NAME(S) AND ADDRESS(ES)

NASA Langley Research Center
Hampton, VA 23681-2199

8. PERFORMING ORGANIZATION REPORT NUMBER

L-20405

9. SPONSORING/MONITORING AGENCY NAME(S) AND ADDRESS(ES)

National Aeronautics and Space Administration
Washington, DC 20546-0001

10. SPONSOR/MONITOR'S ACRONYM(S)

NASA

11. SPONSOR/MONITOR'S REPORT NUMBER(S)

NASA/TM-2014-218259

12. DISTRIBUTION/AVAILABILITY STATEMENT

Unclassified - Unlimited
Subject Category 35
Availability: NASA CASI (443) 757-5802

13. SUPPLEMENTARY NOTES

14. ABSTRACT

This report will present details of a Pressure Sensitive Paint (PSP) system for measuring global surface pressures on rotorcrtaft blades in simulated forward flight at the 14- by 22-Foot Subsonic Tunnel at the NASA Langley Research Center. The basics of the PSP method will be discussed and the modifications that were needed to extend this technology for use on rotor blades. Results from a series of tests will also be presented as well as several areas of improvement that have been identified and are currently being developed for future testing.

15. SUBJECT TERMS

Global pressure measurement; Optical diagnositcs; Pressure sensitive paint; Rotorcraft; Temperature sensitive paint

16. SECURITY CLASSIFICATION OF:			17. LIMITATION OF ABSTRACT	18. NUMBER OF PAGES	19a. NAME OF RESPONSIBLE PERSON
a. REPORT	b. ABSTRACT	c. THIS PAGE			STI Help Desk (email: help@sti.nasa.gov)
U	U	U	UU	41	19b. TELEPHONE NUMBER *(Include area code)* (443) 757-5802

Standard Form 298 (Rev. 8-98)
Prescribed by ANSI Std. Z39.18